A Nanopatterned Cantilever Device for Assaying Contractile Properties of Stem Cell-Derived Cardiomyocytes

Daniel Chen Lih

A thesis

submitted in partial fulfillment of the

requirements for the degree of

Master of Science

University of Washington

2016

Committee:

Deok-Ho Kim

Nathan Sniadecki

Program Authorized to Offer Degree:

Bioengineering

University of Washington

Abstract

A Nanopatterned Cantilever Device for Assaying Contractile Properties of Stem Cell-Derived Cardiomyocytes

Daniel Chen Lih

Chair of the Supervisory Committee:

Dr. Deok-Ho Kim

Bioengineering

Drug-induced cardiotoxicity has been a major issue for both patients and pharmaceutical companies. Current *in vitro* cardiotoxicity screening utilizes genetically modified cell lines, which do not recapitulate adult human cardiomyocytes in terms of their biochemical and electro-physical phenotype. More recently screening technologies have utilized single-cell assays based on human stem cell-derived cardiomyocytes; however, measurements from single cells are incapable of predicting the cardiotoxic effects of drugs at the tissue level. The discrepancy in cell characteristics between *in vitro* culture and native human myocardial tissue has resulted in the release of potentially lethal drugs and the loss of potentially valuable drugs. To improve the accuracy and efficacy of preclinical cardiotoxicity screening, efforts have been made to create *in vitro* assays that measure the cardiomyocytes' contractility, in order to better represent the overall response of the heart to drug treatment.

Here we present a device for assaying the contractile properties of stem cell-derived cardiomyocytes using flexible, nanopatterned cantilevers and aligned cardiac tissue inspired by the structure of native myocardial tissue. Studies have shown that the nanoscale extracellular-matrix fibers play an important role in the alignment, development, and function of native heart tissue. We demonstrate a greater extent of cell alignment and cytoskeletal alignment as compared to unpatterned cantilevers thereby more closely mimicking native tissue structure. This demonstrates the benefits of nanopatterns in guiding the development of cardiomyocytes *in vitro*. We also investigated the contractile development of cantilevers over time and in response to treatment with a known cardiotoxic drug. By characterizing the stress of cantilevers in response to cardiomyocyte contraction, a more direct representation of how cardiotoxicity affects the functionality of cardiac tissue is realized.

ACKNOWLEDGMENTS

I would like to express my deep gratitude to Dr. Deok-Ho Kim, my advisor. He has mentored and supervised my progress throughout my undergraduate and graduate years. During both difficult and successful times of research, Dr. Kim always supported me to achieve the highest standards of my project. Under his guidance, I have learned to take a major role in different research projects. I am grateful to the opportunities he has provided me. I would also like to thank Nathan Sniadecki, a member of my thesis committee and faculty in the department of Mechanical Engineering. Dr. Sniadecki is extremely resourceful and supportive. He provided me great advices in planning future experiments and troubleshooting when problems arose.

Alec Smith, my primary mentor, provided me tremendous support in technical and organizational aspects of my project. Whenever I ran into setbacks, Alec always worked out a plan of action with me. Paulos Yohannes Mengsteab had supported my growth as an independent researcher through training of specific skills and providing advices and help. Eunpyo Choi helped improved multiple figures as well as data analysis. Jesse Macadangdang provided me stem cell-derived cardiomyocytes and NRVMs for experiments and along with Winnie Leung, they assisted me in immunofluorescence staining and confocal imaging. Alex Jiao assisted me with PDMS modification and problem solving. Nisa Penland assisted me with C2C12 differentiation and culturing. Sam Frankel provided me assistance on data analysis. Hao Ding and Camille Biggins provided me with NRVMs for experiments. Young-Soo Choi helped resolved the adhesion issues. Zeid Nawas assisted in the fabrication of devices. Jon

Casamayor performed thickness measurement and SEM images.

I also received supports from other labs. Josh Buser, a graduate student in Yager Lab, was incredibly generous to assist me with laser cutting and cutting designs. Katlyn Gerbin, a graduate student in Murry Lab, instructed me how to perform electrical stimulation.

Finally, I would like to thank my family and friends. My parents, JJ and Suhling, have supported me to achieve my dream of being a bioengineer. They have contributed to my academic and personal development by always being there for me. My brother, Andrew, has been my inspiration and support through all kinds of challenges. Without their unconditional caring and support, I would not be where I am right now.

TABLE OF CONTENTS

TABLE OF FIGURES

CHAPTER 1: INTRODUCTION

1.1 Motivation and Objectives

It has been found that 45% of drug recalls from 1994 to 2006 were due to cardiotoxicity, indicating the wide spread nature of the problem[1]. For example, Fen-phen, an anti-obesity drug, was first introduced in the 1970s. In 1996, it was found that fen-phen caused valvular heart disease. Later in 1997, it was removed from the market. The withdrawal and legal damages associated with this withdrawal cost the company of over $13 billion[2].

Recently, there has been an exponential growth in antitumor drug development. However, due to the specific signaling-pathway targeting properties of these antitumor drugs, many of them are highly cardiotoxic[3]. An analysis on drug development in pharmaceutical companies reveals high cost in phase II and III due to unprecedented nature of drug targets being pursued and stricter drug safety[4]. There is a need to reduce the debilitation from those processes during drug development. By creating a high throughput and cheap drug-induced cardiotoxicity-screening assay, the matter in question could possibly be alleviated. Drug-induced cardiotoxicity screening is therefore an important aspect in drug development and public safety.

Current *in vitro* cardiotoxicity screenings utilize genetically transformed cell lines such as Chinese hamster ovary (CHO) or human embryonic kidney (HEK) cells with expression of single cardiac ion channels. However, these cells do not recapitulate adult human cardiomyocytes in terms of their biochemical and electrophysiological phenotype[5]. The discrepancy in cellular characteristics between *in vitro* assays and

native human myocardial tissue could lead to false negative and false positive results[6,7]. Although promising studies have been conducted using human stem cell-derived cardiomyocytes (hSC-CMs), these single cell experiments, that measure electrophysiological responses to cardiotoxic compounds, do not completely recapitulate the responses of adult human myocardium to drugs in terms of myocardial functions. Moreover, many of the hSC-CMs are developmentally immature resembling fetal cardiomyocytes biochemically and electrophysiologically. There is a great need for a more accurate drug-induced cardiotoxicity-screening assay. Lab efforts have prioritized creating nanoscaled structures that are able to induce and enhance cardiomyocyte development. In order to create a well-developed cardiac tissue, we focus on creating an assay using flexible, biocompatible, nanopatterned cantilevers. The cantilevers are hypothesized to induce well-aligned cardiomyocytes that respond to cardiotoxic drugs by producing differential contractile forces. A direct representation of how cardiotoxicity affects the overall functionality of cardiac tissue could be demonstrated by comparing the contractile characteristics between drug-treated and drug-free cantilevers.

1.2 Background

1.2.1 Heart Structure

The human hearts are composed of helical layers of orderly aligned myocardial fibers. This architecture is crucial to the functions of hearts: contraction and relaxation[8]. The aligned myocardial fibers were made of elongated cardiomyocytes and anisotropically

aligned extracellular matrix (ECM) fibers as shown by previous *ex vivo* studies[9]. The orientation of the cardiomyocytes has been shown to strongly correlate with the direction of the alignment of the underlying ECM fibers[9]. This alignment with the three-dimensional micro- and nano-scaled structures of the heart produced directional contractions using well-paced and spatially-directed electrical signals[10]. The ECM fibers of the heart are made of stretchable collagen and elastin fibers. The elastic modulus of heart tissues ranges from 10 kPa to 60 MPa[11,12]. Biomimetic approaches have been attempted to reproduce the structure of native heart, however, due to its complexity, a tissue-engineered heart has not been completely achieved yet.

1.2.2 Drug-Induced Cardiotoxicity and Current Drug Screening Systems

Drug-induced cardiotoxicity is a major risk in drug development and public safety. The U.S. Department of Health and Human Services (HHS) estimated that nearly 1 million patients suffer from adverse drug reactions each year of which drug-induced arrhythmia is the leading cause[13]. In order to identify potential cardiotoxic drugs before market release, both the U.S. Food and Drug Administration (FDA) and pharmaceutical companies have started to implement mandatory preclinical drug screening. Current *in vitro* cardiotoxicity screenings have used genetically transformed cell lines such as CHO or HEK cells that expressed a single type of cardiac ion channels. The genetically transformed cells have not been able to accurately recapitulate genetic, cellular, biochemical, or electrophysiological properties of native human myocardium[14]. Specifically, those assays have focused on screening for compounds that prolong the QT interval through blockade of the hERG potassium channel. However, assays relying

on hERG potassium channel blockade have frequently produced false negative and false positive results[6,7]. As an alternative, animal heart models have also been utilized in cardiotoxicity screening. It is important to note that animal cardiomyocytes have different electrophysiological properties comparing to human cardiomyocytes, thus responding differently to certain drugs[15,16]. There is a great need for an improved drug-induced cardiotoxicity-screening method.

1.2.3 Stem Cell Maturity

As shown in several *in vitro* disease-modeling studies, induced pluripotent stem cell (iPSC) derived- neurons, hepatocytes, endothelial cells, and cardiomyocytes have been developmentally immature and have not been able to completely reproduce the physiological properties of their adult counterparts *in vivo*[17-20]. For example, human induced pluripotent stem cell-derived cardiomyocytes (hiPSC-CMs) have demonstrated incomplete calcium-handling ability in their sarcoplasmic reticulum, thus imperfectly recapitulating electrophysiological output of adult cardiomyocytes[20].

Only a portion of the number of the ion channels expressed in adult cardiomyocytes *in vivo* have been verified to be present in hiPSC-CMs indicating developmental immaturity of hiPSC-CMs as compared with adult cardiomyocytes[14]. Both human embryonic stem cell-derived cardiomyocytes (hESC-CMs) and hiPSC-CMs have been better characterized as resembling human fetal cardiomyocytes as opposed to adult cardiomyocytes in terms of their genetic expression and electrophysiology[21]. It has been speculated that the immaturity of stem cell-derived cardiomyocytes could be caused by unpatterned and stiff substrates such as culture dishes used in many studies.

As described previously, with patterned and flexible substrates, cardiomyocytes have been shown to align themselves with the patterns with improved electrophysiological functions and myofibrillogenesis[22].

1.2.4 Nanotopography

It is important to note that substrates with proper nano-architecture have been able to control cell shapes, mechanics, and functions, such as growth, differentiation, migration, and gene expression. Inspired by the architecture of native human-myocardium fibers, nanotopographic cues were utilized to guide the alignment and development of cardiac tissue *in vitro* (**Figure 1**). Previous studies by Kim *et al*. have shown the benefits of nanopatterns to the development of cardiac tissue *in vitro*. Specifically, they have demonstrated nanopatterned substrates were able to induce alignment of cardiomyocytes in the same direction as the direction of the nanopatterns. The alignment has also been observed at the subcellular level as shown in the cytoskeletal structures such as microfilaments and sarcomeres. Moreover, the nanopatterns has been shown to induce higher rate of electrophysiological and mechanical coupling among the cultured cardiomyocytes as indicated by higher action potential propagation speed in the direction of the nanopatterns[9]. Nanotopography with 800 nm groove widths has been shown to be the optimal dimension for cardiomyocyte alignment and development[23-25].

1.2.5 PDMS Mechanical Properties

Polydimethylsiloxane (PDMS) has been shown to possess great hemocompatibility, biocompatibility, and little inflammatory behaviors in *in vivo* studies making it a suitable material for cell culturing[26]. Cell adhesion on PDMS has been a problem due to PDMS's hydrophobicity and quick recovery from hydrophilic treatment. However, multiple methods have been developed to extend the treatment or permanently modify the surface chemistry, enhancing long-term cell adhesion[27-31].

Studies have shown that the patterning ability of PDMS is limited between 500 and 800 nm while the resolution could be improved by hardening the PDMS[32,33]. Moreover, the elasticity of PDMS have been shown to range from 0.6 to 3.5 MPa depending on the ratio of base and curing agent mixed and the temperature and time baked[34-36]. PDMS is highly stretchable and is able to bear repeated stretching. Together, the mechanical properties of PDMS fall within the range of the mechanical properties of native human myocardium making PDMS a great substrate for cardiac tissue engineering[37].

1.2.6 Relevant Studies: Stem Cell-Derived Cardiomyocytes and Cardiotoxicity

hiPSC-CMs and hESC-CMs have been utilized to create assays for drug-induced cardiotoxicity screening. The results have demonstrated that disease-specific hiPSC-CMs be used to elucidate clinical susceptibilities of high-risk populations to drug-induced cardiotoxicity[14]. Moreover, the cardiotoxicity of certain arrhythmic compounds was recapitulated by inducing the hypertrophy-cardiomyopathy phenotypes in hESC-CMs[38]. The use of patient-specific hiPSC-CMs to detect cardiotoxicity is more accurate

and predictive compared to the use of genetically modified HEK cells.

Multiple previous works have demonstrated cardiotoxic effects of drugs on hiPSC-CMs. In Himmel's study, mouse embryonic stem cell-derived cardiomyocytes (meSC-CMs) and hiPSC-CMs were utilized as models to assess the effects of cardiotoxic drugs. The electrophysiological responses of meSC-CMs and hiPSC-CM to compounds, that have been characterized previously in terms of their effects, such as hERG K^+ channel blockers and trafficking inhibitors, slow delayed rectifier K^+ channel blockers, Na^+ channel blockers and gating inhibitors, L-type Ca^{2+} channel blockers, and Na–K-ATPase inhibitors, were investigate. As expected, meSC-CMs and hiPSC-CMs responded distinctively to the drugs. However, the responses also differed from the established *in vitro* and *in vivo* models. Detailed characterizations indicated a mixed fetal and adult gene expression in both cell lines. The drug-induced cardiotoxicity may be detected with the system; however, the predictive or translational value was likely limited and not established[39].

Sirenko *et al.* utilized calcium-sensitive dyes to detect calcium flux changes, allowing the monitoring of beating rate, amplitude, and other parameters of the electrophysiological properties of stem cell-derived cardiomyocytes. Positive chronotropes which include β1- and β2-adrenoreceptor antagonists, such as epinephrine and isoproterenol, were used. Negative chronotropes which include propranolol, a nonselective β-blocker, doxazosin, a β1-adrenoreceptor blocker, verapamil, an L-type calcium channel blocker, and acetylcholine, an acetylcholine receptor agonist, were used. Concentration-dependent changes in beat rate were

observed and were in agreement with the mode of action of each compound[40]. hiPSC-CMs together with a low-impedance microelectrode array (MEA) system have been tested to determine its benefits for preclinical cardiotoxicity screening. Navarrete *et al*. showed that the responses of hiPSC-CMs to drugs were consistent with reported drug effects in literature qualitatively and quantitatively. Drug-induced arrhythmias were recapitulated in hiPSC-CMs and documented with the MEA[21].

The systems described previously only focused on electrophysiological properties and did not fully recapitulate other important properties of cardiomyocytes, such as contractile properties. Furthermore, the stem cell-derived cardiomyocytes used in these studies were developmentally immature and did not represent adult human cardiomyocytes as described previously[14,21].

1.2.7 Cantilevers

Several studies have made use of thin PDMS substrates to investigate the contractile properties of cardiomyocytes. You *et al*. has utilized neonatal rat ventricular myocytes (NRVMs) grown on micropatterned PDMS thin film to investigate cardiac physiology by varying cantilever shapes and drug treatments. Contraction stress is dependent on surface topography and types of drug treatments[41].

Several groups have utilized micro-contact printed fibronectin on PDMS thin film of different shapes to create constructs that represent actuators and powering devices using NRVMs[42,43]. McCain *et al*. has shown a similar construct made with micro-contact printed fibronectin on gelatin thin films[44]. The thin films have also been utilized in striated muscle contractility assays ("muscle on a chip")[45]. Most importantly, the micro-

contact printed ECM proteins on PDMS thin films have been used to create a ‘‘heart on a chip’’ to measure contractility, action potential propagation, and cytoskeletal architecture. The chip was able to measure structure-function relationships of cardiac tissues[46]. Deflection of these thin films during muscle contraction allowed for the calculation of diastolic and systolic stresses generated by the engineered tissues using modified Stoney’s question[47,48]. Together with studies of gene expression, morphology, and electrophysiology, cardiomyocytes can be characterized in almost all aspects[49,50].

It is important to note that even though micropatterned and micro-contact printed substrate are able to guide the alignment of cardiomyocyte in the micro-scale level, it does not resemble the native heart tissue structurally. Specifically, because micro-patterns and micro-contact printing include features with sizes similar to one single cell, they work by constricting cells to the patterned area. On the other hand, nanopatterns are usually smaller than a single cell. Nanopatterns might induce cellular responses through a more fundamental mechanism such as receptor signaling[51].

1.3 Summary

In summary, current *in vitro* assays, using genetically transformed cell lines, for drug-induced cardiotoxicity screening are ineffective giving false negative and false positive readings. Efforts to improve the accuracy of such assays have led researchers to use stem cell-derived cardiomyocytes in hope of better recapitulating adult human cardiomyocytes. Substrates with microscale features were also utilized in hope of better recapitulating native human myocardium. However, the immaturity of stem cell-derived

cardiomyocytes and the structural discrepancy of engineered cardiac tissue from that of native heart tissue have limited their screening ability. In order to improve the maturity of cardiomyocytes, we created nanopatterns on flexible PDMS surfaces to mimic the structural and mechanical properties of adult human myocardium *in vivo*. Stress produced by cardiomyocytes could be demonstrated by the deflection of cantilevers and directly quantified using established methods. We hypothesized that the nanopatterned cantilevers could provide a more physiologically resembling evaluation of the contractile properties of cardiomyocytes than flat cantilevers. If the nanopatterned cantilevers successfully demonstrated improved assaying abilities, our cantilevers could be employed for drug-induced cardiotoxicity assays, which would provide more accurate readings comparing to the current drug screening systems. They could also be utilized in disease modeling to study disease processes and potential medical interventions.

1.4 Thesis Outline

In this thesis we develop nanopatterned cantilevers for assaying contractile properties of cardiomyocytes by quantifying cell layer stresses. We will characterize the structural and mechanical properties of cantilevers and optimize cell attachment using multiple cell lines. We will investigate the effects of nanopatterns on cardiomyocytes and the behaviors of cantilevers under different conditions such as before and after drug treatment.

In chapter 2, we demonstrate the ability to create PDMS cantilevers with an optimized stiffness, thickness, nanopatterns, and sizes. Eventually, cantilevers with

desired properties are created reproducibly. We also demonstrate that the cantilevers are able to support cell adhesion before and after cantilever release using C2C12.

In chapter 3, we demonstrate cell alignment and structural maturity induced by nanopatterns. We observe the responses of different cell lines including, NRVM and hESC-CMs, to nanopatterned PDMS cantilever. Cell alignment, cytoskeletal alignment, and structural maturity are analyzed.

In chapter 4, cantilevers and cardiomyocytes are combined to perform drug-induced cardiotoxicity testing. We propose to determine the ability of the cantilevers to assay contractile properties of stem cell-derived cardiomyocytes and detect the cardiotoxic effects of known cardiotoxic compounds by analyzing cantilever deflection. In chapter 5, we present our conclusions of the studies as well as ongoing and future works.

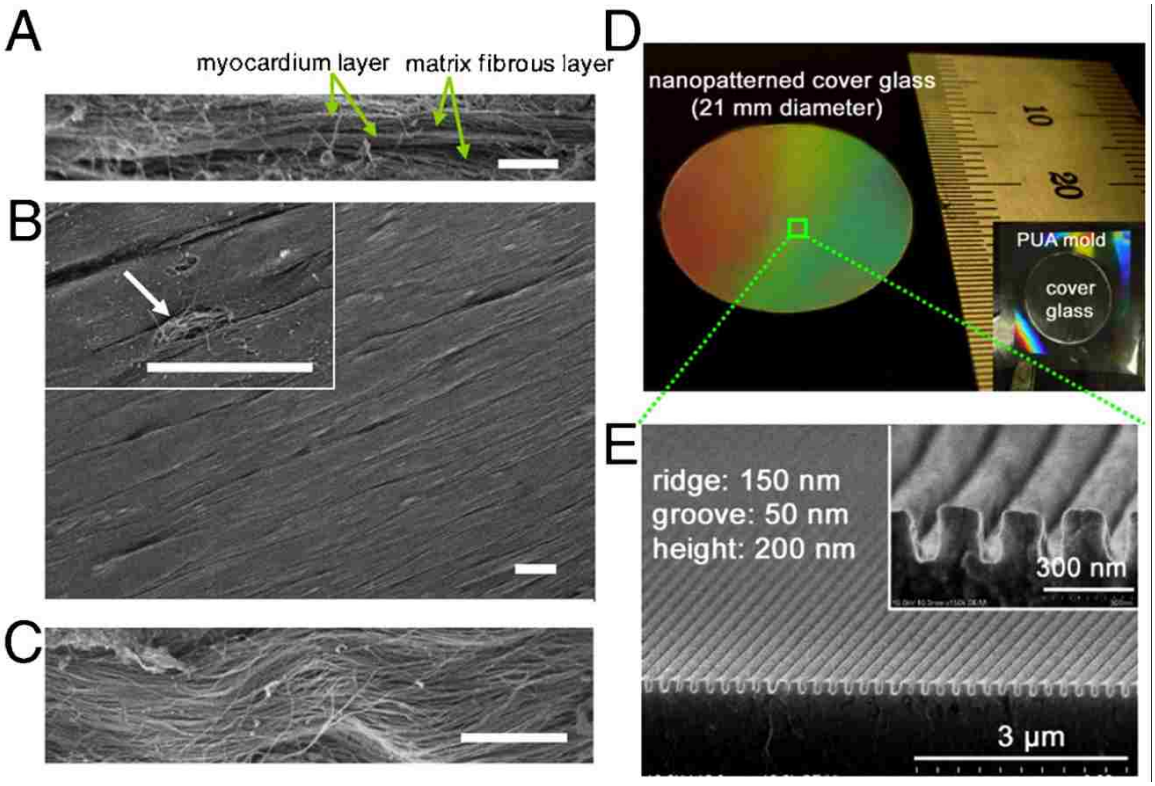

Figure 1. Nanopatterned substrates fabricated to mimic native cardiac tissue structures. (A-C) SEM images of *ex vivo* heart tissue of adult rat heart showing fiber alignment. (D) Nanopatterned substrate fabricated on a glass coverslip. (E) SEM image of the nanopatterned substrate. [Scale bar: 5 μm in (A); 10 μm in (B) and (C)]. *Kim, et al., PNAS, 2010. 107(2): p. 565-570*.

CHAPTER 2: STRUCTURAL, MECHANICAL, AND CELLULAR CHARACTERIZATION OF CANTILEVERS

2.1 Introduction

In a previous study by Grosberg *et al.*, stress quantification was performed on deflecting PDMS thin films with contracting cardiomyocytes. In order to perform stress quantification with nanopatterned cantilevers made in our lab, we would need to replicate what have been done with the equipment available in our lab. Cantilevers were fabricated at different conditions and settings and characterized using scanning electron microscope (SEM). The first endpoint of the project was to optimize the conditions and setting for device fabrication and attain the desired nanotopography and thickness. We hypothesized that we would be able to create cantilevers with identical nanopatterns and thicknesses reproducibly with our optimized protocols.

Before we were able to obtain cantilever deflection from cellular contraction, we wanted to ensure that cells were able to adhere on PDMS cantilevers before and after cantilever release. Cell adhesion has always been an issue on PDMS substrates, so various methods to improve cell adhesion to PDMS were investigated. In this study, we would also focus on extending cell adhesion on the cantilevers. Cell adhesion studies were conducted using C2C12, a mouse-myoblast cell line. The reasoning behind this decision was impacted by our available resources and accessibility in our immediate lab. We hypothesized that the modified PDMS substrates would be able to enhance cell adhesion and support long-term cell culture.

2.2 Materials and Methods

2.2.1 Silicon Master and PUA Mold

A silicon wafer with nanopattern of ridge of 800 nm, groove of 800 nm, and height of 600 nm was used as the master for creating second-generation molds. Second generation mold made with polyurethane acrylate (PUA, MINS 301 RM, Minuta Technology) was prepared. Briefly, the silicon master was cleaned with isopropanol and dried with clean dry air. A few drops of PUA solution was pipetted on the silicon wafer, and a polyethylene terephthalate (PET, Skyrol®, SKC) film was place on top. The PUA solution slowly spread out as a result of capillary action. The solution was then flattened and bubbles were removed using a roller. It was placed in fusion cure system (Minuta Technology) for 1 minute. The PET film was then separated from the silicon wafer and cured under UV light overnight.

2.2.2 PDMS Mold

PDMS mixture was prepared by mixing the base and curing agent (Sylgard 184, Dow Corning) in a 10-to-1 ratio then the bubbles were removed by placing in desiccator in vacuum. On a square petri dish (100 mm by 100 mm, VWR), the PUA mold was tightly taped at the bottom. The PDMS mixture was then poured into the petri dish to cover the PUA mold. Excessive bubbles were removed by vacuum again. It was cured overnight at 65 °C in an oven (Model 1410, VWR). After curing, the PDMS was cut around the edge of PUA mold with a razor blade and peeled off to get the PDMS mold. In order to reduce adhesion between the mold and newly fabricated devices, treatment with silane was required[52,53]. Briefly, PDMS mold was cleaned with a stream of air and plasma

treated at 80 W, 0.5 Torr for 5 minutes in O_2 plasma machine (Femto Science). In the fume hood, 125 µL of (tridecafluoro-1, 1, 2, 2, -tetrahydrooctyl)-1-trichlorosilane (Sigma-Aldrich) was pipetted and transferred into a small glass vial (20 mL, Sigma-Aldrich). The interior of a desiccator was covered with aluminum foil to prevent coating on the interior surface of the desiccator. The vial of trichlorosilane and PDMS mold were placed in the desiccator and they were vacuumed with a small pump (Model 15500, Robinair) for 20 minutes. The desiccator was sealed and pump was turned off. The set up was allowed to stand for 2 hours in fume hood. Trichlorosilane treated PDMS mold could be used multiple times for molding. Disposables contacted with trichlorosilane was disposed by wrapping in foil and placing in the biohazard bin due to its toxicity.

2.2.3 Glass Coverslip and Spin Coating

Glass coverslips (25 mm diameter, Fisher Scientific) were washed in ultrasonic cleaner (Model 2510, Bransonic) for 1 hour in isopropyl alcohol (Pharmco-aaper) and individually blown dry with air. The coverslips were then spread side-by-side on a piece of paper and were plasma treated at 100 W, 0.5 Torr for 5 minutes in O_2 plasma machine (Femto Science). Plasma treated coverslips should be used immediately because the surface modification was temporary. The coverslips were taped onto the center of a circular petri dish using removable tape (Scotch). Four pieces of removable tape were taped around the coverslip creating a small window (about 1 cm by 1 cm) at the center of the coverslip (**Figure 2A**). The petri dish along with the coverslip was placed and adhered on a spin coating machine (Model WS-400BZ- 6NPP/LITE, Laurell Technologies Corporation). 80 µL of 10% w/v poly(N-isopropylacrylamide) (PNIPAM,

Polyscience, Inc.) in 1-butanol (Fisher Scientific) was pipetted onto the square window on the coverslip. The coverslip was spin coated at 6000 rpm for 1 minute (**Figure 2B**). The four pieces of tape was carefully removed from the coverslip. 400 µL of PDMS 10:1 mixture was pipetted on top of the PNIPAM layer and was spin coated at 4000 rpm for 1 minute (**Figure 2C**). The coverslip was carefully removed from the petri dish.

2.2.4 Soft Lithography and Curing

The spin coated coverslip was cured at 65 °C in oven for 1 hour and transferred to a leveled surface with the PDMS layer facing up. An adhesion-reduction treated PDMS mold was placed on top of the coverslip with patterned side facing down for 30 minutes (**Figure 2D**). The set up was vacuumed in a desiccator with a vacuum pump for 30 minutes. The set up was removed from the desiccator and if mold was not completely in contact with the PDMS layer of the coverslip, the mold was gently pressed to enhance contact. The set up was cured overnight at 65 °C in oven. Finally, the PDMS mold was separated from the coverslip (**figure 2E and 2F**).

2.2.5 Laser Cutting

A 10.6-micron wavelength CO_2 laser prototyping system (VersaLaser 2.0, 10 W, Universal Laser Systems, Scottsdale, AZ) was used to create cantilevers. 70% ethanol was used to sterilize all equipment and tools that came in contact with the devices to minimize contamination. An acrylic board of 20 cm diameter was used as a template for cutting allowing multiple coverslips to be cut at once. Coverslips were taped onto the acrylic board in a 4 by 4 array. Laser cut was performed at 2% power and 7% speed.

Three cantilevers were produced for each coverslip. Specifically, a rectangular snake-shaped line of 1 mm width was created forming three 2 mm by 5 mm cantilevers (**Figure 3A and 3B**). In cellular experiments, cells were seeded on the cantilevers and the edge was later peeled off (**Figure 3C – 3E**).

2.2.6 Cantilever Characterization

Cantilevers were characterized in terms of the topography and thickness with SEM equipment was available on the University of Washington – Washington Nanofabrication Facility (UW WNF). Thickness was also measured using bright field images from an optical microscope (Eclipse Ti-E, Nikon).

2.2.7 PDMS Surface Modification and Protein Coating

The pre-laser cut devices were washed in warm DI water overnight and dried in oven overnight. First, PDMS surface of the devices was plasma treated at 80 W, 0.5 Torr for 5 minutes in O_2 plasma machine (Femto Science). In order to enhance cell adhesion to PDMS, PDMS surface modification was performed using oxygen plasma[31], silane[54], positive peptide[30,55], and ECM proteins[29] (**Figure 4**). The devices were sterilized under UV for 15 minute. 500 µL of warm 1% v/v (3-glycidyloxypropyl) trimethoxysilane (GPTMS, Sigma-Aldrich) in water was pipetted onto PDMS surface of the devices. The devices were incubated at 37 °C for 20 minutes in an incubator. The devices were washed with warm DI water for 3 times. 500 µL of warm 100 µg/mL poly-D-lysine hydrobromide (PDL, Sigma-Aldrich) was pipetted onto PDMS surface of the devices followed with a 1-hour incubation at 37 °C. The devices were washed again with warm DI water for 3 times. Devices were dried at 37 °C for about 10 to 20 minutes. Finally,

500 µL of 0.1% gelatin was pipetted onto the devices to cover desired PDMS surface. Devices were incubated at 37 °C overnight for protein adsorption. The devices could be stored in 4°C until future experiment.

2.2.8 PDMS Filling and Device Assembly

PDMS mixture was prepared by mixing the base and curing agent (Sylgard 184, Dow Corning) in a 10-to-1 ratio. About 3 g of the mixture was poured into a 35-mm petri dish then the bubbles were removed by placing in a desiccator in vacuum. The PDMS was cured overnight and separated from the petri dish the next day. A 1 cm-by-1.5 cm rectangle hole was created at the center of the circular PDMS disk using a razor blade to create the PDMS filling. PDMS fillings were then submerged in methanol overnight and in DI water for another night. The PDMS filings were cleaned with Kim wipes and placed in bio-safety cabinet for drying and UV sterilization for least one night. The PDMS fillings were adhered with the laser-cut cantilever devices by pressing the PDMS side of cantilever device together with the bottom of PDMS filling (**Figure 5A and 5C**). The adhered parts were loaded into a sterile 35-mm petri dishes or a 6-well plate (**Figure 5B**).

2.2.9 C2C12 Culture and Seeding

Mouse myoblast cell line, C2C12, was cultured and passaged with the already established protocol[56]. Briefly, C2C12 were cultured in Dulbecco's Modified Eagle Medium (DMEM, high glucose + glutamine, no sodium pyruvate, Gibco), 10% FBS, and 1% Penicillin-Streptomycin (Pen-Strep) in culture flasks pre-coated with 0.1% gelatin.

Once the confluency of C2C12 myoblasts approached 100%, C2C12 myoblasts were replated to cantilever devices pre-coated with 0.1% gelatin at 300,000 cells/cm^2. Culture was maintained in differentiation medium composed of DMEM (high glucose + glutamine, no sodium pyruvate, Gibco), 2% horse serum, 1 ng/mL insulin, and 1% Pen-Strep in incubator at 37 °C and 5% CO_2. Medium was changed every 48 hours until further procedures. Cell attachment and myotube formation were monitored with optical microscope daily. Phase-contrast images were taken with the optical microscope (TS100F, Nikon).

2.3 Results and Discussions

2.3.1 Cantilever Nanopattern and Thickness

The results obtained from this study agreed with what has been previously reported[53]. By following the adhesion reduction protocol, we were able to produce different patterns using different silicon masters without mold-substrate separation issues. Specifically, PDMS cantilevers with 20 μm (data not shown) or 800 nm groove widths (**Figure 6**) were fabricated reliably. The reproducibility was validated with SEM images by confirming the dimensions of the patterns on the cantilevers (**Figure 6**).

A closer investigation of spin coating speed and thickness was conducted with SEM. With SEM imaging the thickness of the nanopatterned PDMS cantilevers was measured 22 μm thick at 3000 rpm, 17.2 μm at 3250 rpm, and 16.1 μm thick at 3500 rpm. Another set of thickness data was obtained using an optical microscope. In agreement with the literature[57], we observed decreasing PDMS layer thickness with

increasing spin coating speed (**Figure 7**). Cantilever thickness measured using SEM images was consistently less than the reported value of 20 μm at 4000 rpm[57]. The difference could be explained by additional pressure applied on the PDMS during the soft lithography and curing processes. There also existed a nonlinear relationship between thin film thickness and spin coating speed[57].

2.3.2 Mechanical Properties of Cantilevers

It is important to note that the mechanical properties of cantilevers were affected by many factors. For example, higher curing temperature and longer curing time both increase the stiffness of PDMS. The structures of cantilevers, such as the thickness and shape, could also alter the mechanical properties. Topography could also be an important factor. Flat cantilevers were unpatterned while nanopatterned cantilevers consisted of anisotropically aligned troughs and ridges on one of its surface. We were able to analytically characterize the bending moments and the moments of inertia of both cantilevers[58]. With the same amount of shear force, the bending moment of nanopatterned cantilever was about 1.53% greater than that of flat cantilever. The moment of inertia of nanopatterned cantilever is about 4.86% greater than that of flat cantilever. Together, to obtain the same amount of cantilever deflection, the nanopatterned cantilever needed 3.28% more force than that of flat cantilever.

2.3.3 Cell Adhesion on Cantilevers

We used C2C12 to investigate the interaction between cells and cantilevers due to its availability in the lab. With the PDMS surface modification using plasma, silane, and

peptide, cell adhesion was greatly improved as shown by comparing two C2C12 experiments (**Figure 8**). Cell adhesion was maintained during the most of the course of culture. With non-beating C2C12, monolayer was maintained for more than 20 days after cell seeding on cantilevers. Formation of aligned myotubes was also observed in multiple experiments indicating proper culturing conditions for the C2C12 (**Figure 8B**).

Other interactions of cells with cantilevers were investigated, specifically, the behaviors of cells before and after release of cantilevers. The first problem encountered was the inability of cantilevers to release from glass. We discovered that cells were able to grow over and under the laser cut locking cantilevers in place (**Figure 9A**). This could be explained by the order of PDMS cantilever preparation procedures. Laser cut was performed before PDMS surface modification. Silane and peptide used in PDMS modification could possibly diffuse into the laser cut. As a result, fibronectin was coated on the laser cut increasing cell adhesion at the cut site. In order to circumvent this problem, we tried cutting PDMS layer by hand with scalpel. We performed multiple trials by hand cut; however, the dimensions and shape of cantilevers were not reproducible (**Figure 10A**). There were also problems with cell detaching from the cantilevers once the cuts were made (**Figure 10A**).

Another possible solution to cantilever affixation was to perform laser cut after all the preparation steps were completed. In this way, we would prevent fibronectin coating over the cut. With this approach, we were able to reduce cell adhesion at the laser cut site while maintaining high cell adhesion on the cantilever (**Figure 9B**). Occasionally, we observed spontaneous cantilever release without cell detachment from the

cantilevers (**Figure 10B**). With this approach, we were able to release cantilevers without perturbing the cell layer.

2.4 Summary

This study aimed to validate our ability to fabricate cantilevers reproducibly and enhance cell adhesion on PDMS. Using SEM and optical imaging, we were able to verify the thickness and topography of cantilevers. We were able to reproduce identical nanopatterns following the optimized protocol. However, variations in PDMS substrate thickness and elasticity were observed. A PDMS thickness within the range of 16 to 20 μm was created. Further studies on thickness distribution in relation to spin coating speed and mechanical properties of cantilevers from different batches of devices are required.

Cell adhesion study was performed using a mouse myoblast cell line because it was readily available in our lab. We were able to greatly enhance C2C12 adhesion on PDMS by chemically modifying the surface of PDMS. However, C2C12 behave very differently from cardiomyocytes. Considering that cardiomyocytes do not secrete copious amount of ECM onto their underlying substrate, cardiomyocytes generally are not able to support cell adhesion themselves. It is important to note that C2C12 adhesion might not directly translate to cardiomyocyte adhesion.

Cantilever release was another important aspect to be considered before we were able to quantify force generation from cells. By performing laser cut as the last step of cantilever preparation, we prevented cantilever affixation caused by overgrown

cells and avoided manual procedures that could perturb the cell layer. In summary, we demonstrated a system in which cells were able to remain adhered while cantilevers were released from the coverslip.

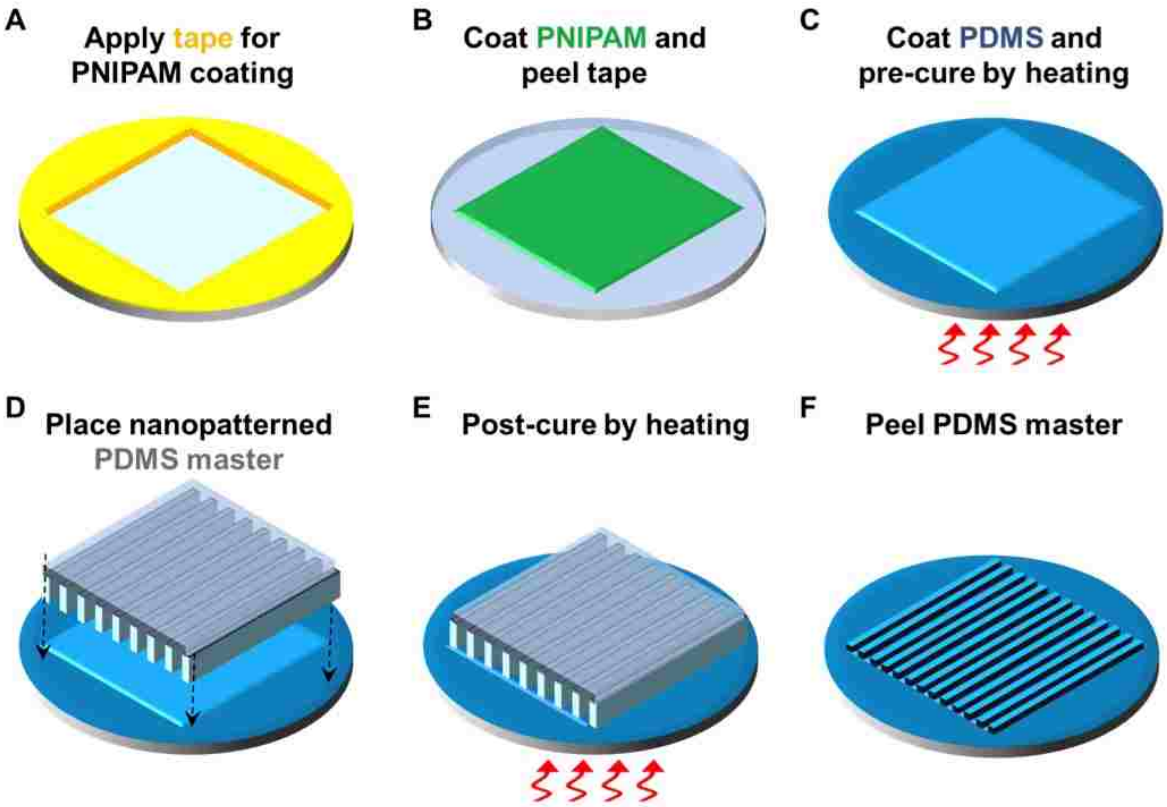

Figure 2. Schematics of the fabrication procedures of nanopatterned PDMS device. (A) 4 pieces of removable tape were applied to form a square window at the center of a glass coverslip. (B) PNIPAM was applied and spin-coated and tapes were removed creating a square-area coated with PNIPAM. (C) PDMS was spin-coated on top of PNIPAM and pre-cured at 65 °C. (D) After 1 hour pre-cure at 65 °C, a nanopatterned PDMS mold was applied on top of the PDMS. (E,F) After overnight curing at 65 °C, PDMS mold was removed and the nanopatterned PDMS device was created.

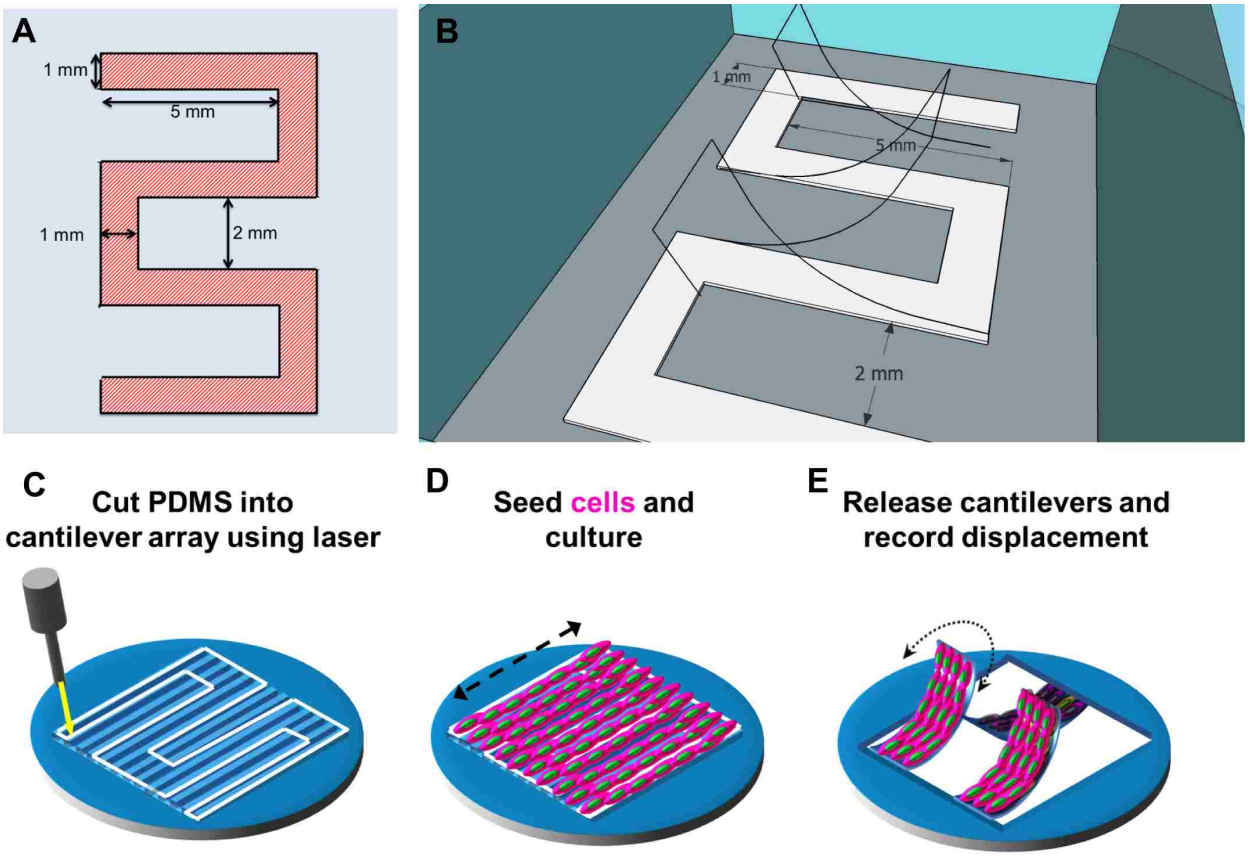

Figure 3. Schematics showing 3 cantilevers created with laser cut on a PDMS device. (A) Black lines surrounding the red-shaded area represent laser cut. The red-shaded area represents the area that would be peeled off after PNIPAM is dissolved at 32 °C. Each cantilever is a 5-by-2-mm rectangle. (B) Isometric view of released cantilevers. (C) Laser cut was performed within the area of nanopattern. (D) Cells were seeded on the pattern. (E) The edge of cantilevers was peeled off allowing for the release of cantilevers.

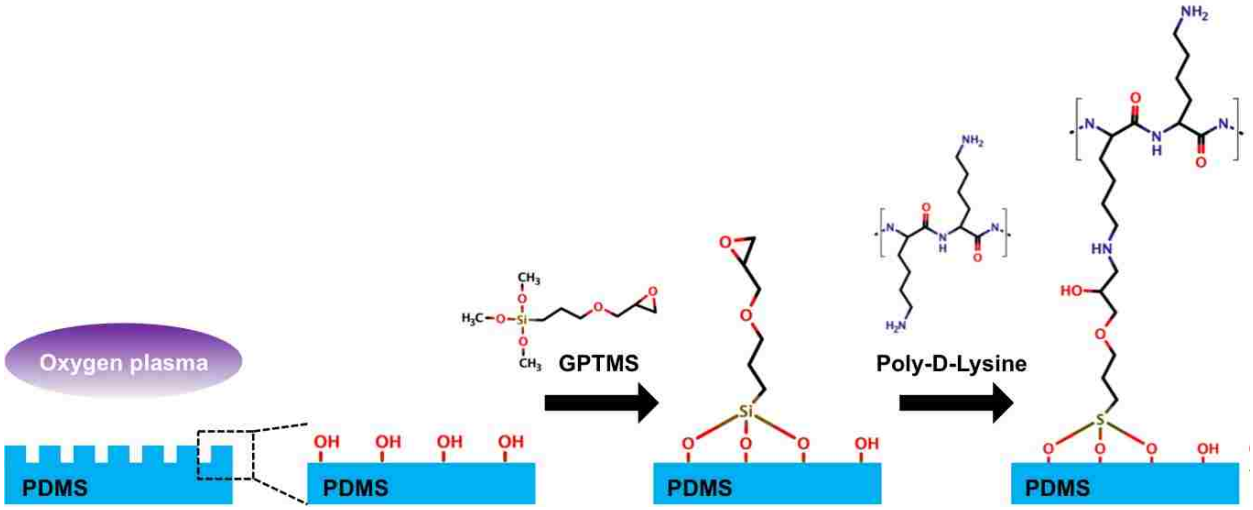

Figure 4. PDMS surface modification to enhance cell adhesion. PDMS is first treated with oxygen plasma to create silanol groups on the surface. GPTMS is introduced and reacts with the silanol groups to form epoxy-terminated functional groups. PDL reacts with epoxy and is covalently bonded to the functional group. ECM proteins are adsorbed onto the positively charged PDL functionalized surface.

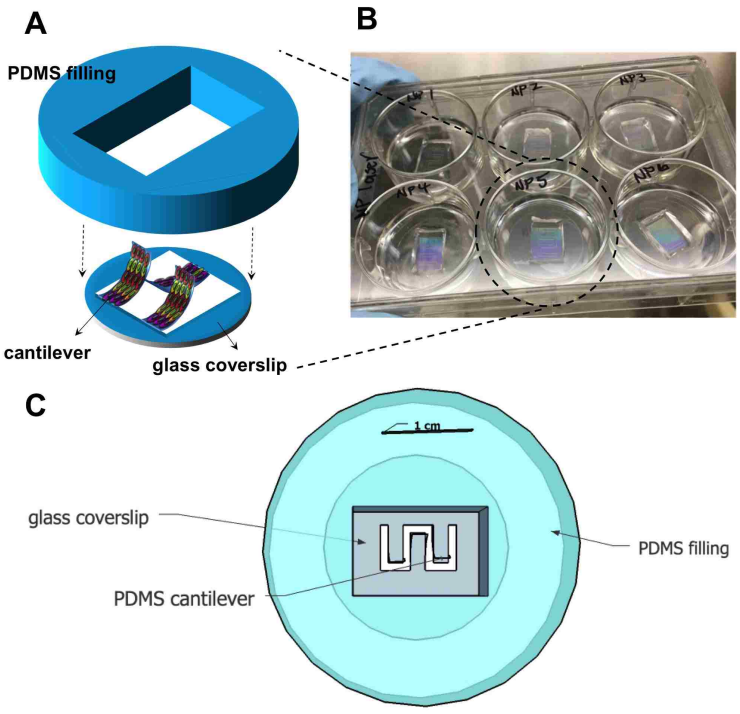

Figure 5. Schematics of cantilever devices used in cell culture. (A) Isometric view of cantilever device before assembly. (B) Assembled devices were loaded into a 6-well plate. (C) Top view of cantilever device after assembly. PDMS filling allowed for minimizing medium used for cantilever experiments.

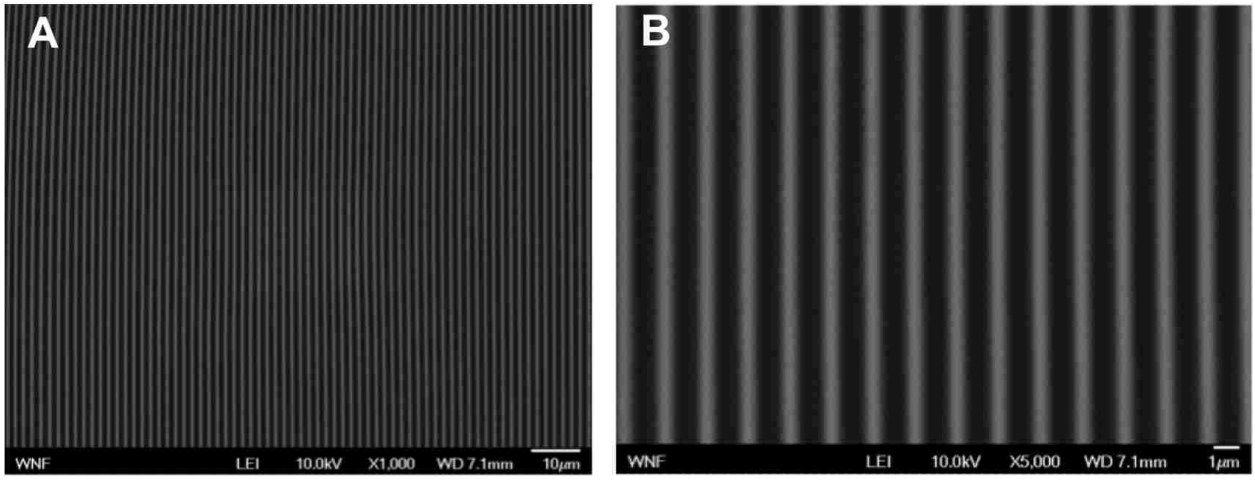

Figure 6. SEM images of nanopatterns with 800 nm groove widths on PDMS devices. (A) 1000x SEM magnification showing the extensiveness of the nanopattern. (B) 5000x SEM magnification of the nanopattern showing well aligned ridge and groove structures.

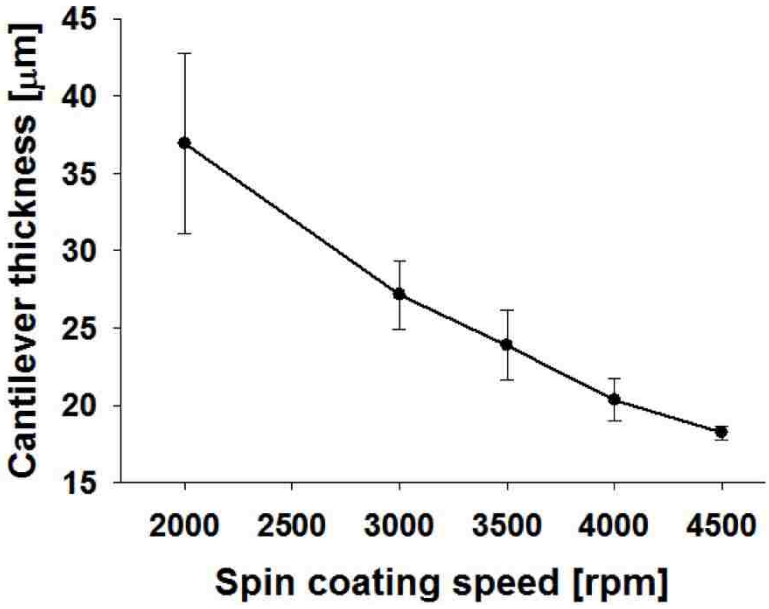

Figure 7. Cantilever thickness measured using optical microscope. The thickness of PDMS cantilevers over a range of spin coating speed was plotted. The thickness decreased as the spin coating speed increased. (Error bars: ± SEM)

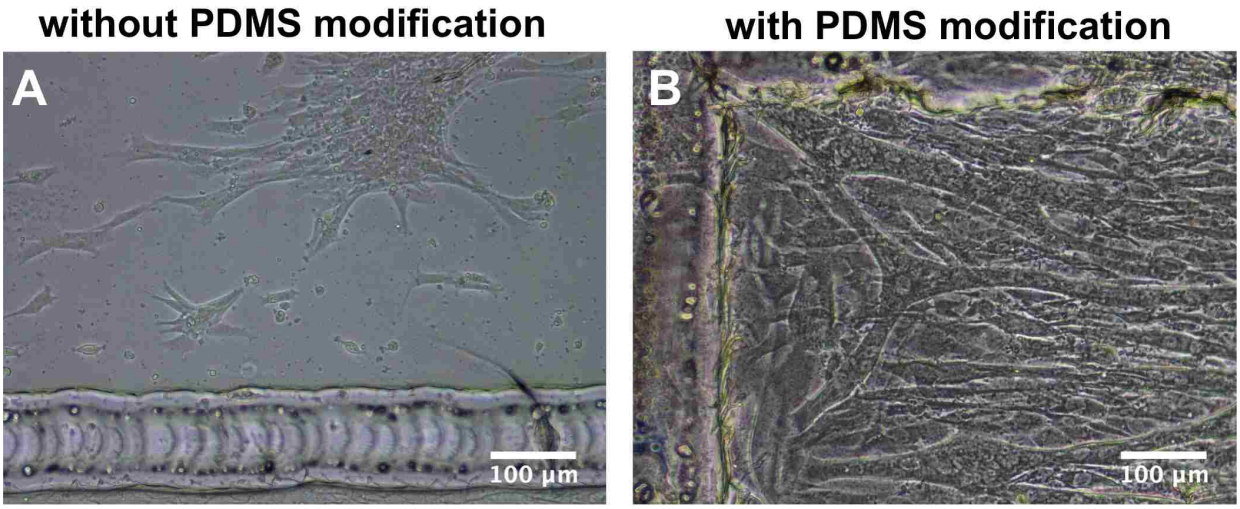

Figure 8. PDMS surface modification was shown to greatly improve C2C12 cell adhesion. (A) Cantilever without PDMS surface modification. (B) Cantilever with PDMS surface modification. Unlike treated devices, very little cell adhesion and significant cell clumping were observed in devices without treatment. Myotube formation was observed on the treated devices.

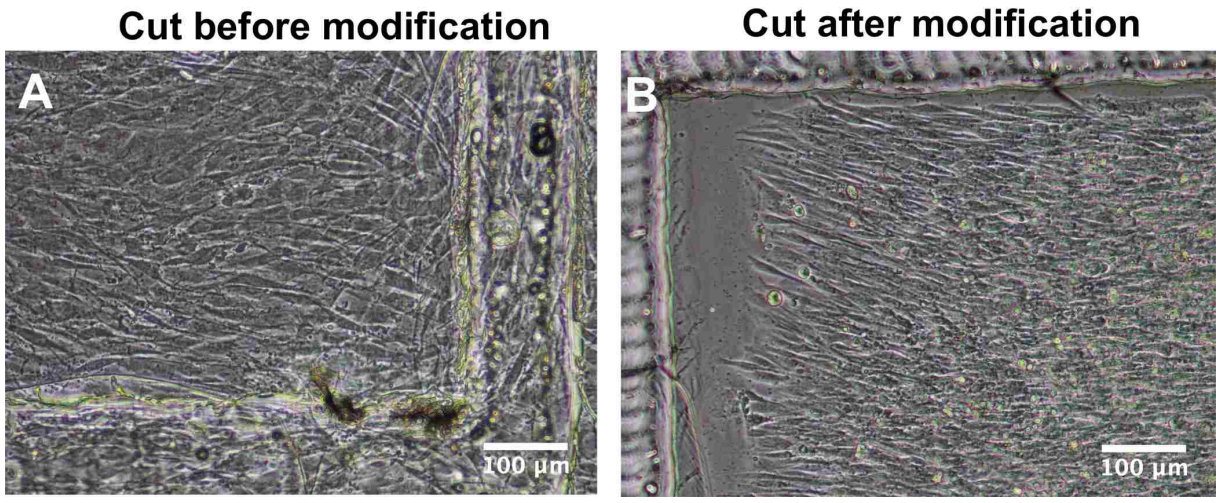

Figure 9. Cantilever release was improved by performing laser cut after modification. C2C12 growth in proximity to laser cut was dependent on treatment order. (A) When laser cut was performed before PDMS surface modification and ECM protein coating, C2C12 grew over the laser cut inhibiting the release of cantilever. (B) When laser cut performed after all treatment, C2C12 only grew within the area of cantilever.

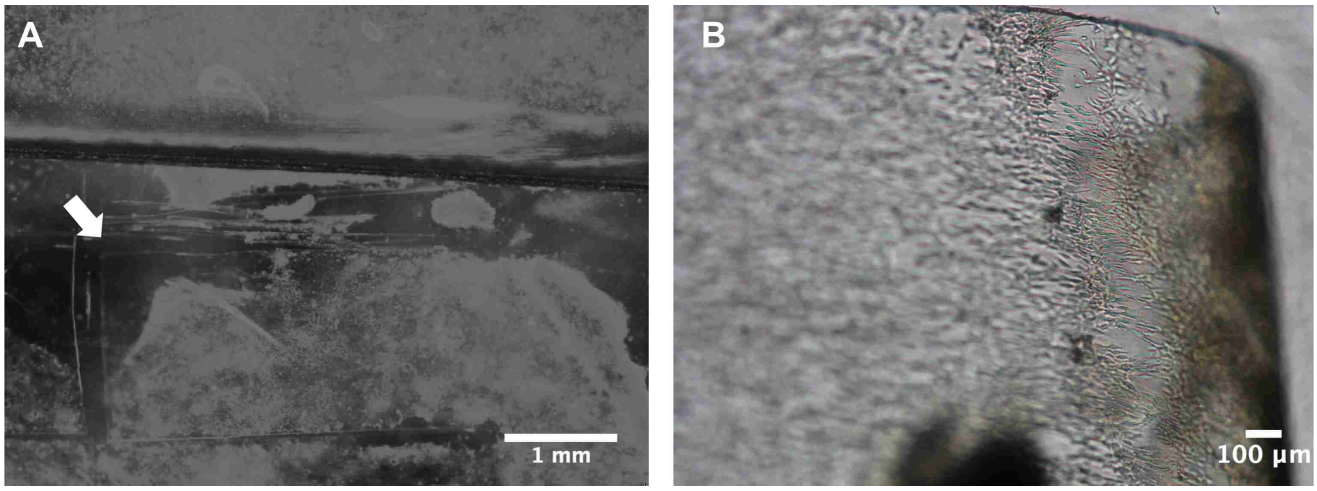

Figure 10. Laser was more reliable in producing clean cut and identical cantilevers. (A) A cantilever created manually using a scalpel in an H7-CM experiment. White arrow indicates messy cut and cell detachment around the upper left corner of cantilever. (B) A cantilever created using laser in a C2C12 experiment. The edge of the cantilever is clean and straight.

CHAPTER 3: CELL ALIGNMENT AND STRUCTURAL MATURATION ON CANTILEVERS

3.1 Introduction

Different topographical and mechanical features are observed in different tissues in the body. The features correlate with the functions of each type of tissue. In tissue engineering, it has been shown that surface properties of substrates affect cell behaviors in terms of morphology, biochemistry, electrophysiology, and contractility. Specifically, certain topography and elasticity of the substrate were shown to improve development and function of certain cell type[59]. Nanoscaled topography and elasticity in megapascal range have been demonstrated to be optimal for cardiac tissue development and function as shown by more mature biochemical, structural, electrophysiological, and contractile properties of the stem cell-derived cardiomyocytes[23-25]. In this study, we would use PDMS as the substrate to develop cantilevers owing to its ability for nanopatterning and its elasticity and stretchability. A previous study has utilized PDMS thin films micro-contact printed with fibronectin in multiple applications validating the feasibility of our design[42].

In this study, we would focus on improving cell alignment to nanopatterns on the cantilevers. Responses such as cell alignment, cytoskeletal alignment, and structural maturity of different cell lines including, NRVM and hESC-CMs, on nanopatterned PDMS cantilevers were expected to be similar. We hypothesized that cells cultured on nanopatterned cantilevers would show a higher degree of alignment and structural maturation than those cultured on flat cantilevers. One way to measure structural

maturation of cardiomyocytes is to quantify its sarcomere length. Sarcomere length is directly related to force production from cell contractions. It has been reported that adult cardiomyocytes have sarcomere lengths in the range from 2.1 to 2.3 um while immature cardiac cells have sarcomere lengths of 1.5 um[60]. We used sarcomere length as an indicator for maturity. We also wanted to demonstrate the ability of cells to remain on cantilevers once cantilevers were released from glass.

3.2 Materials and Methods

3.2.1 PDMS Surface Modification and Protein Coating

The cantilever devices were made as described in chapter 2. They were washed in warm DI water overnight and dried in oven overnight. PDMS surface of the devices was plasma treated at 80 W, 0.5 Torr for 5 minutes in O_2 plasma machine (Femto Science). In order to enhance cell adhesion to PDMS, PDMS surface modification was performed using oxygen plasma[31], silane[54], positive peptide[30,55], and ECM proteins[29]. The devices were sterilized under UV for 15 minutes. 500 µL of warm 1% v/v (3-glycidyloxypropyl) trimethoxysilane (GPTMS, Sigma-Aldrich) in water was pipetted onto PDMS surface of the devices. The devices were incubated for 20 minutes in incubator at 37°C. The devices were washed with warm DI water for 3 times. 500 µL of warm 100 µg/mL poly-D-lysine hydrobromide (PDL, Sigma) was pipetted onto PDMS surface of the devices followed with a 1-hour incubation at 37°C. The devices were washed again with warm DI water for 3 times. Devices were dried in incubator for about 10 to 20 minutes. Finally, 500 µL of 50 µg/mL fibronectin (Sigma-Aldrich) was pipetted to cover desired PDMS surface. Devices were then incubated at 37°C overnight for protein adsorption. The

devices could be stored in 4°C until future experiment.

3.2.2 Laser Cutting

A 10.6-micron wavelength CO_2 laser prototyping system (VersaLaser 2.0, 10 W, Universal Laser Systems, Scottsdale, AZ) was used to create cantilevers. 70% ethanol was used to sterilize all equipment and tools that came in contact with the devices to minimize contamination. An acrylic board of 20 cm diameter was used as a template for cutting allowing multiple coverslips to be cut at once. Coverslips were taped onto the acrylic board in a 4 by 4 array. Laser cut was performed at 2% power and 7% speed. Three cantilevers were produced for each coverslip. Specifically, a rectangular snake shaped line of 1-mm width was created forming three 2-mm-by-5-mm cantilevers.

3.2.3 PDMS Filling and Device Assembly

PDMS mixture was prepared by mixing the base and curing agent (Sylgard 184, Dow Corning) in a 10-to-1 ratio. About 3 g of the mixture was poured into a 35-mm petri dish then the bubbles were removed by placing in desiccator in vacuum. The PDMS was cured overnight at 65°C and separated from the petri dish the next day. A 1-cm-by-1.5 cm-rectangle hole was created using a razor blade at the center of the circular PDMS disk to create PDMS filling. The PDMS fillings were submerged in methanol overnight and in DI water for another night. The PDMS filings were cleaned with Kim wipes and placed in bio-safety cabinet for drying and UV sterilization for least one night. The PDMS fillings were adhered with the laser cut cantilever devices by pressing the PDMS side of cantilever device together with the bottom of PDMS filing. The adhered parts

were then loaded into a sterile 35 mm petri dishes or a 6-well plate.

3.2.4 NRVM Seeding and Culture

Prior to NRVM seeding, the PDMS was modified and coated with fibronectin and cut using laser. NRVMs were obtained from two-day-old Sprague–Dawley rats (Harlan) following previous methods[9]. NRVMs were seeded with a density of 2,040 cells/mm^2 approximated from 1 million cells on 25-mm diameter coverslip as described[42]. NRVMs were then cultured in media consisted of 4 parts of DMEM (high-glucose, -sodium pyruvate, Invitrogen) and 1 part of M199 (Lonza), HEPES (17 mM, Sigma-Aldrich), 10% horse serum (Gibco), 5% fetal bovine serum (Sigma-Aldrich), and 1% Pen-Strep (Invitrogen). 10 μM of Ara-C (Sigma-Aldrich) was used to eliminate proliferating cells such as fibroblasts to achieve a higher cardiomyocyte purity[61,62]. Culture was maintained in incubator at 37°C and 5% CO_2. Medium was changed every 48 hours until further procedures. Cell attachment and growth was monitored with optical microscope (TS100F, Nikon) daily. Phase-contrast images and videos were taken with the optical microscope.

3.2.5 RUES2-CM Differentiation, Seeding, and Culture

Human embryonic cell line, RUES2, was used for generating cardiomyocytes. Cardiac differentiation was accomplished using an established protocol in the lab. Replated RUES2 cells were induced with Roswell Park Memorial Institute (RPMI) Medium 1640 (Gibco) supplemented with B-27 (Gibco) plus supplemental 100 ng/mL of activin A. After 24 hours the activin A containing medium was replaced with RPMI/B27 with

supplemental BMP-4 and cultured for 4 days without medium change. At day 5, bone morphogenetic protein 4 (BMP-4) containing medium was replaced with RPMI/B27 medium. After day 5 cells were fed with RPMI/B27 medium every other day and monitored for spontaneous beating activity which peaked around day 14. The differentiated cardiomyocytes were then fed until replating for cantilever experiments between days 18 and 20. Prior to RUES2 derived-cardiomyocyte (RUES2-CM) seeding, the PDMS was modified and coated with fibronectin and cut using laser. RUES2-CMs were replated to cantilever devices using plating medium containing RPMI/B27, 10% FBS, and 1:1000 ROCK inhibitor to minimize apoptosis. Cells were seeded at 150,000 cells/cm^2. Culture was maintained in incubator at 37 °C and 5% CO_2. Medium was changed every 48 hours until further procedures. Cell attachment and growth was monitored with optical microscope (TS100F, Nikon) daily. Phase-contrast images and videos were taken with the optical microscope.

3.2.6 H7-CM Differentiation, Seeding, and Culture

Human embryonic cell line, H7, was used for generating cardiomyocytes. Cardiac differentiation was accomplished using an established protocol[63]. Cells were differentiated similar to RUES2 cardiac differentiation with the addition of 5 ng/mL basic fibroblast growth factor (bFGF) between day 1 to day 4, 10 ng/mL of vascular endothelial growth facto (VEGF) between day 4 to 8 and both between day 8 to 14. The differentiated cardiomyocytes were then fed until replating for cantilever experiments between days 18 and 20. Prior to H7 derived-cardiomyocyte (H7-CM) seeding, the PDMS was modified and coated with fibronectin and cut using laser. H7-CMs were

replated to cantilever devices using plating medium containing RPMI/B27, 10% FBS, and 1:1000 ROCK inhibitor to minimize apoptosis. Cells were seeded at 150,000 cells/cm^2. Culture was maintained in incubator at 37 °C and 5% CO_2. Medium was changed every 48 hours until further procedures. Cell attachment and growth was monitored with optical microscope (TS100F, Nikon) daily. Phase-contrast images and videos were taken with the optical microscope and saved.

3.2.7 Cell Elongation and Orientation Analysis

With phase-contrast images, the outline of cells was manually traced using ImageJ (National Institute of Health). Using an elliptical best fit, the major and minor axes could be identified. Cell elongation was calculated as the ratio of the lengths of its major axis to minor axis. Orientation was calculated based on the angle of ellipse's major axis in relation to a determined axis, where 0° indicated alignment to the axis[9].

3.2.8 Immunofluorescence staining and Confocal Imaging

Cells were washed with PBS for 5 minutes twice. 100 µL of 4% paraformaldehyde was then added to fix the cells at room temperature for 15 minutes. Cells were washed with PBS for 1 minute for three times. Paraformaldehyde waste was disposed in properly labeled waste bottle. Cells were permeabilized with 0.1% PBS-Triton-X100 for 5 minutes twice. Cells were blocked with 1% bovine serum albumin (BSA) in PBS for 1 hour at room temperature. Cells were incubated in primary antibody α-actinin diluted by 1000 in 1% serum overnight at 4°C. Cells were washed with 0.1% PBS-Triton-X100 for 10 minutes twice the next day. Light was avoided in he following steps. The conjugation

of 1° & 2° anti-bodies was done by adding Alexa 594 goat anti mouse and phalloidin 488 (both diluted by 100) and incubated for 1 hour at 37 °C. Cells were washed in 1mL of PBS for 5 minutes. Nucleus staining was done by adding 2 drops of Vectashield + DAPI to each sample. The sample was sealed with nail polish. Samples were stored in 4C until imaging. Confocal imaging was done on a confocal microscope (Model LSM 510 Meta, Zeiss Confocal Microscope) located at South Lake Union – UW medicine.

3.2.9 Cytoskeletal Alignment and Sarcomere Length Analysis

Fluorescent images of F-actin fibers of cardiomyocytes were analyzed for alignment using custom-made MATLAB scripts. Sarcomere length analysis was performed using confocal images of cells stained with anti-actinin and the respective secondary antibody. The profiles along multiple single myofibril fibers were taken with MATLAB (MathWorks). The profiles were processed with customs-made program in our lab. Average sarcomere length for each sample was calculated.

3.2.10 Electrical Stimulation

Electrical stimulation was performed using 6 well carton electrode cartridges from IonOptix with the C-Pace EP Culture Stimulation System (CEPSYS) (IonOptix)[64]. Cells were subjected to stimulation for a short period of time to induce synchronized contraction. Stimulation parameters used were 20 V for amplitude, 1 Hz for frequency, 15 ms for duration[65,66].

3.2.11 Statistical Analysis

All data are presented as mean ± SEM unless specified otherwise. Student's t-test was used to evaluate the statistical significance between different experimental groups. Significance level was set at $p < 0.05$.

3.3 Results and Discussion

We were able to create monolayer on multiple cell lines early in the culture. Unlike C2C12, monolayer of beating cardiomyocytes rarely persisted past one week after cell seeding on cantilevers. Usually around 7 days after seeding, cardiomyocytes began to detach from cantilevers and form cell aggregates **(Figure 11C and 11F)**. This could be explained by cardiomyocytes' contractile nature. Over time, cardiomyocytes would pull themselves off from a surface that does not support long-term cell culture, such as PDMS.

The effects of nanopatterns on every cell line were noticeable. Unlike cells cultured on flat cantilevers, cells cultured on nanopatterned cantilever demonstrated a more ordered growth. On the cellular lever, cells aligned themselves with the underlying nanopattern and cell elongation in the direction of pattern was universal in C2C12 (**Figure 8 and 9**), H7-CMs (**Figure 11D, 11E, and 11F**), and RUES2-CMs (data not shown). Quantitative elongation and orientation analysis also demonstrated a higher degree of cell elongation and alignment to the nanopattern on the cantilevers as opposed to lower cell elongation and random alignment of cells on the flat cantilevers (**Figure 12**). Using immunofluorescence staining and confocal microscope, we were

able to observe alignment of cytoskeletons in the same direction of nanopatterns showing effects of nanopatterns at the subcellular level. The images of cytoskeletal structures provided both qualitative and quantitative representations of the differences in cell morphology between flat (**Figure 13A, 13B, and 13C**) and nanopatterned (**Figure 13D, 13E, and 13F**) cantilevers. F-actin stress fiber alignment analysis showed a greater extent of cytoskeletal alignment to the underlying nanoapttern (**Figure 14A – 14C**). It is important to note that cells that were stained positive for α-actinin in the NRVM confocal images were patchy indicating problem with the purity of NRVM. The application of fibroblast growth inhibitor (Ara-C) improved the purity of NRVM culture, but there were too little NRVMs left to form a monolayer. Further investigation to improve the quality of NRVM isolation and purity of NRVMs is needed.

By quantifying the sarcomere lengths of cardiomyocytes, we would be able to approximate their maturity level. The sarcomere lengths of NRVMs were compared between NRVMs cultured on flat and nanopatterned cantilevers. We also compared the sarcomere lengths of NRVMs in early and prolonged culture. It was found that on average the sarcomere lengths were about 1.54 (± 0.02) and 1.67(± 0.02) μm for NRVMs cultured on flat and nanopatterned cantilevers over 4 days and 1.87(± 0.03) and 1.92(± 0.05) μm for NRVMs cultured on flat and nanopatterned cantilevers over 25 days. Statistically significant differences in sarcomere lengths were found between NRVMs cultured on flat and nanopatterned cantilevers over 4 days and between NRVMs cultured over 4 and 25 days on either flat or nanopatterned cantilevers. However, we did not observe a statistically significant difference in sarcomere lengths between NRVMs

cultured on flat and nanopatterned cantilevers over 25 days (**Figure 15**). This could be explained by the extended duration of NRVM culture, because the most remarkable differences in sarcomere lengths were usually observed within 7 days after NRVM seeding. The sarcomere lengths of H7-CMs cultured on nanopatterned substrate were significantly greater than those on flat substrate (**Figure 14D**). This difference indicated nanopattern-induced structural maturation. Sarcomere lengths less than 2 μm were detected for all NRVM and H7-CM experiments indicating the cardiomyocytes were not as mature as adult cardiomyocytes. However, all the sarcomere lengths were consistently greater than 1.5 μm indicating enhancement in maturity comparing to immature cardiomyocytes.

The results were consistent with previous studies[23] in which the morphology of the cardiomyocytes became more elongated and aligned, cytoskeletons became more ordered, and sarcomeres became more developed. Future investigation, such as quantification of gene expression and electrophysiological experiments, could further validate the benefits of nanopatterns in enhancing the structural maturation of cardiomyocytes.

3.4 Summary

In this study, we investigated cellular interactions with the topography of PDMS cantilevers. We presented a system that allowed for cell organization and structural maturation. It was shown that cell morphology, specifically elongation and alignment, was consistent with the expectation. Every cell line responded to the nanotopography by

aligning to its underlying substrate pattern. This study also demonstrated cytoskeletal alignment to nanopattern indicating a more fundamental cellular response to topography. Quantification of sarcomere lengths of cardiomyocytes showed improved structural maturity when cardiomyocytes were cultured on nanopatterned cantilevers as opposed to those on flat cantilevers. A prolonged culture time could also improve cardiomyocyte structural maturity. Nanopattern-induced structural maturity was also observed in H7-CM study. The results from both cell line were consistent.

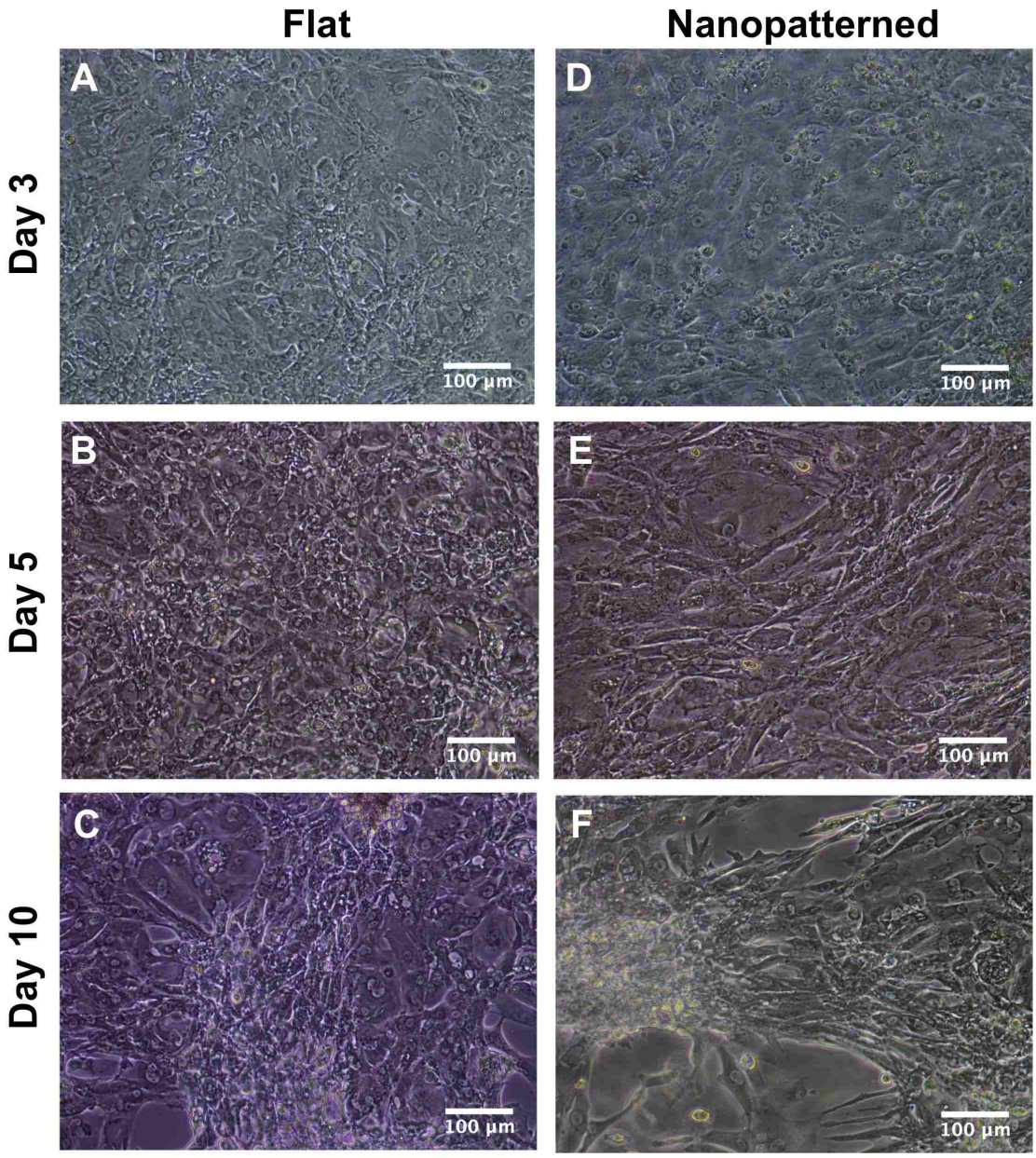

Figure 11. H7-CM monolayer was optimal at day 5. H7-CMs cultured on flat (A,B,C) and nanopatterned (D,E,F) cantilever device at day 3, 5, and 10. Cell detachment and clumping of H7-CMs were observed starting around day 7. Direction of nanopatterns is horizontal.

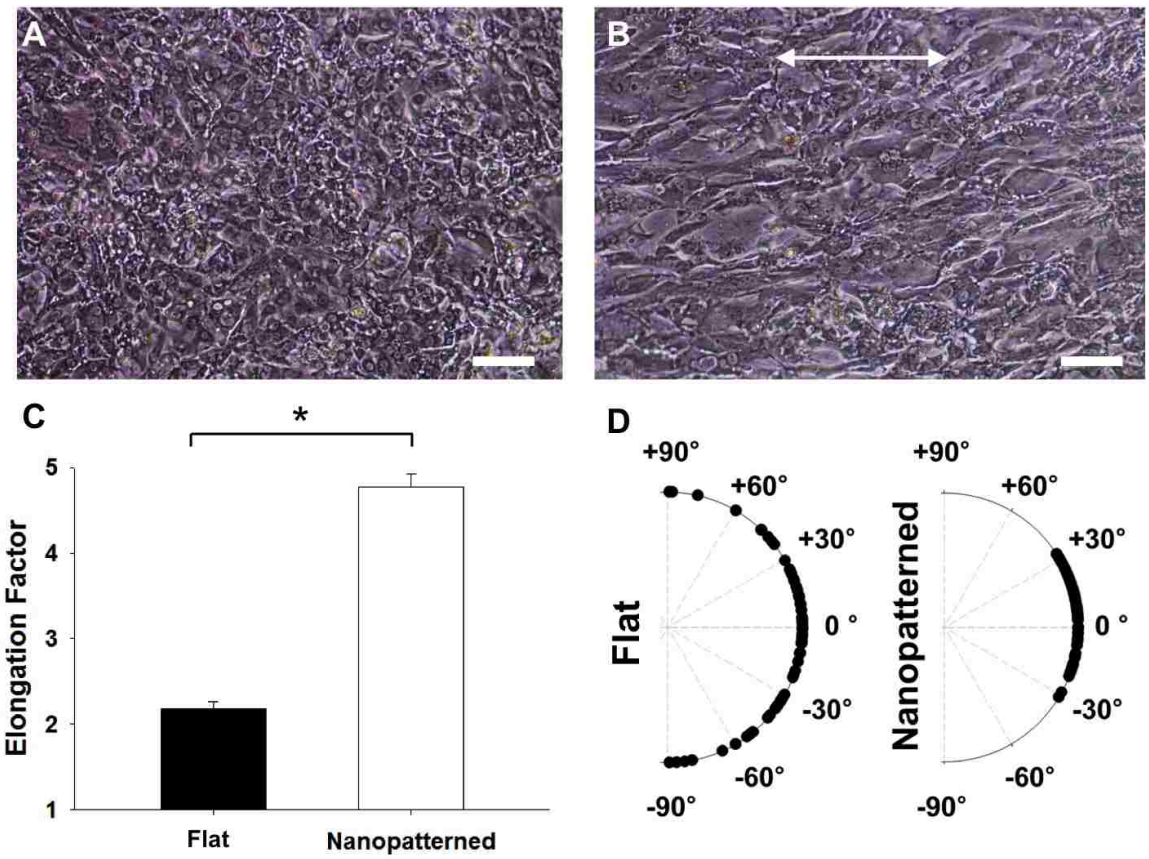

Figure 12. Quantitative cell elongation and orientation analysis of H7-CMs on flat and nanopatterned cantilevers. (A) A phase-contrast image of H7-CMs on flat PDMS substrate at day 5. (B) A phase-contrast image of H7-CMs on nanopatterned PDMS substrate at day 5. (C) Cell elongation of H7-CMs on flat and patterned PDMS substrates (N = 6 images; 12 elongation measured per image; *p < 0.001, error bar: SEM. (D) Quantification of cell orientation on flat and patterned PDMS substrates. Each dot represents a single cell (N = 6 images; 12 angle measured per image. Scale bars: 100 μm in (A) and (B)]

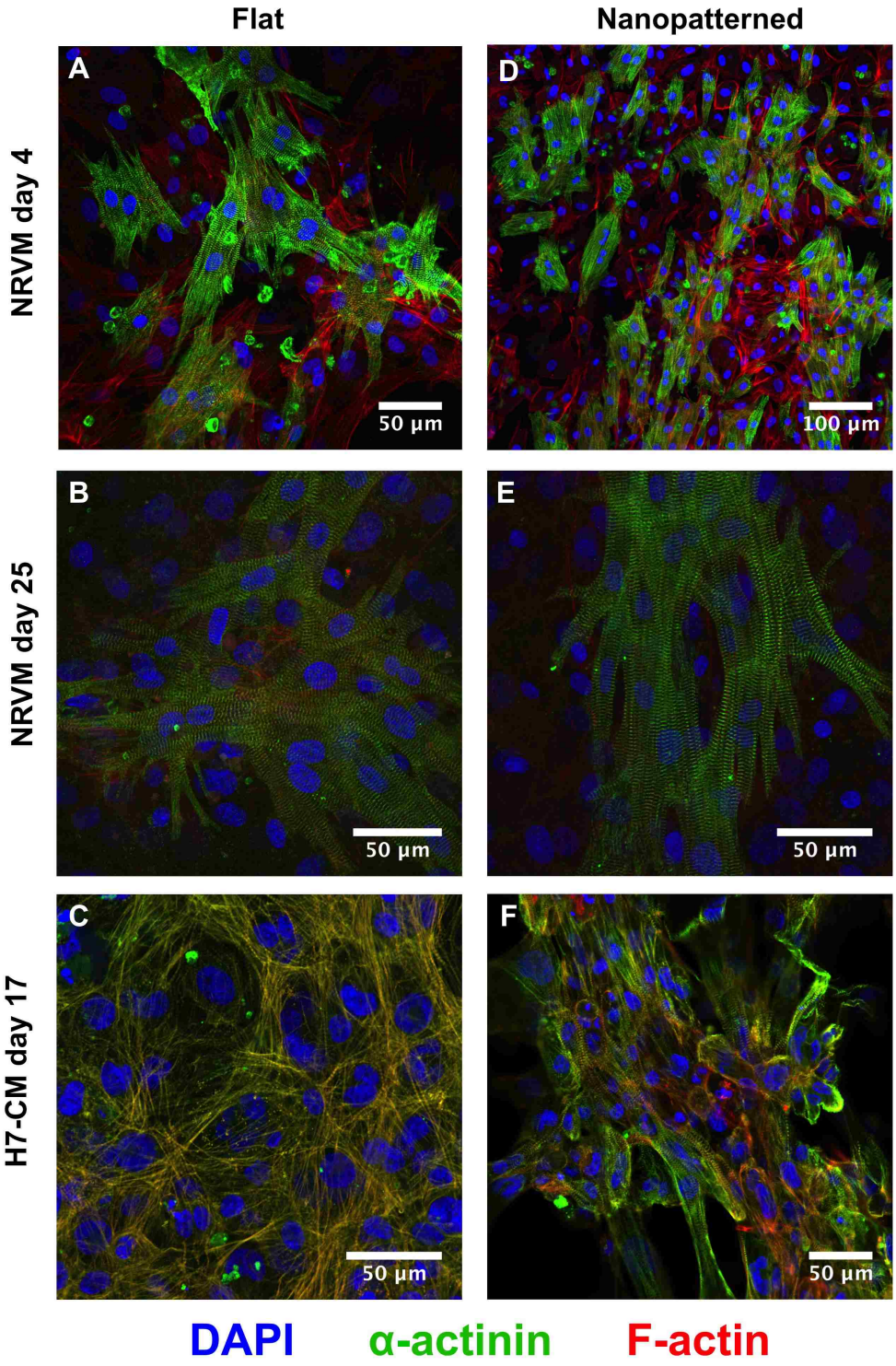

Figure 13. Cytoskeletal structures of NRVMs and H7-CMs were shown to align with their underlying topography. Immunofluorescence confocal images of NRVMs (A,B,D,E) and H7-CMs stained on day 17 (C,F) cultured on flat and nanopatterned PDMS substrates. (A-C) Cells were randomly aligned on the flat substrate. (D-F) Cells aligned in the same direction as the nanopattern. Direction of nanopatterns is vertical.

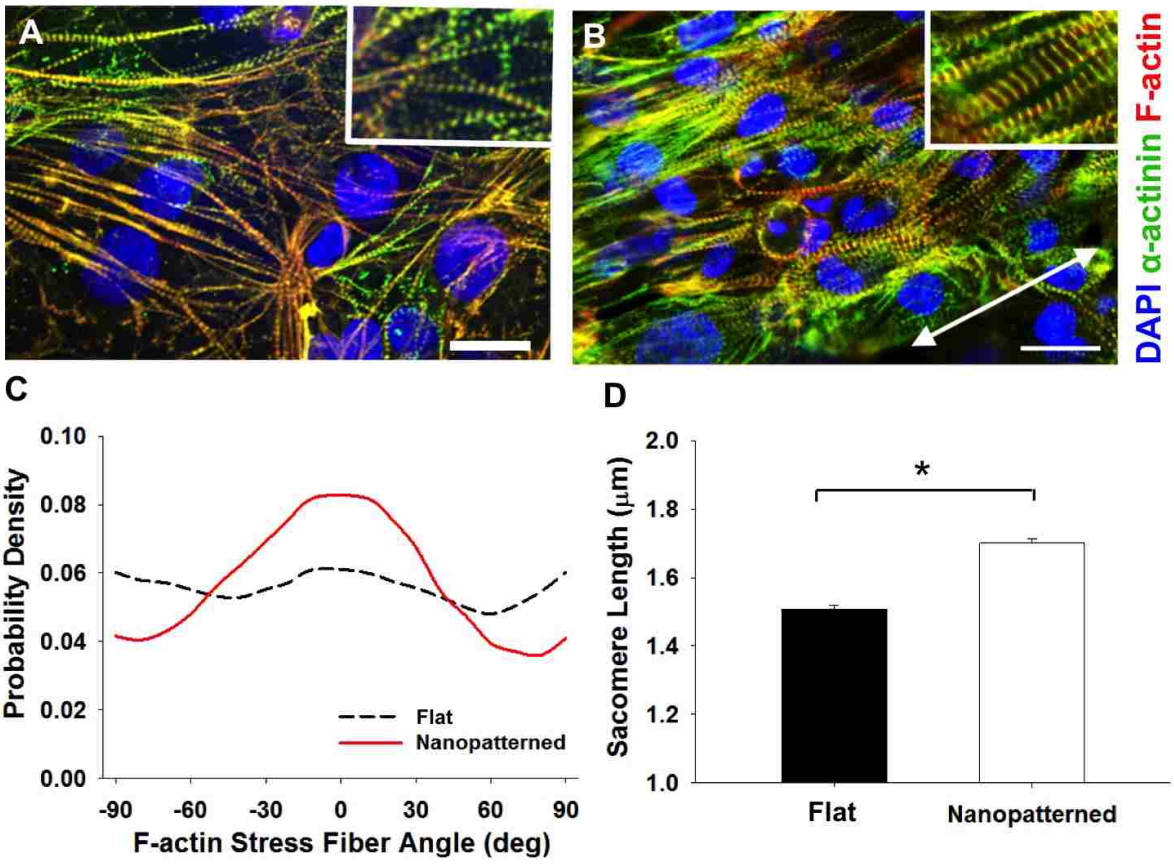

Figure 14. H7-CMs structural analysis on flat and nanopatterned PDMS substrates. (A) H7-CMs cultured on flat PDMS substrate for 17 days. Inset provides close-up detail of sarcomeric structure. (B) H7-CMs cultured on nanopatterned PDMS substrate for 17 days. Inset provides close-up detail of sarcomeric structure. White arrow indicates pattern direction. Scale bars: 25 μm. (C) F-actin stress fiber alignment analysis. Actin fiber orientation was measured and grouped based on their angle relative to the horizontal plane. In all nanopatterned samples, the images were oriented so that the underlying nanotopography ran horizontally. (D) Comparison of sarcomere lengths measured from flat and nanopatterned H7-CMs following 17 days in culture. N = 6 images (100 sarcomeres measured per image), *$p < 0.001$.

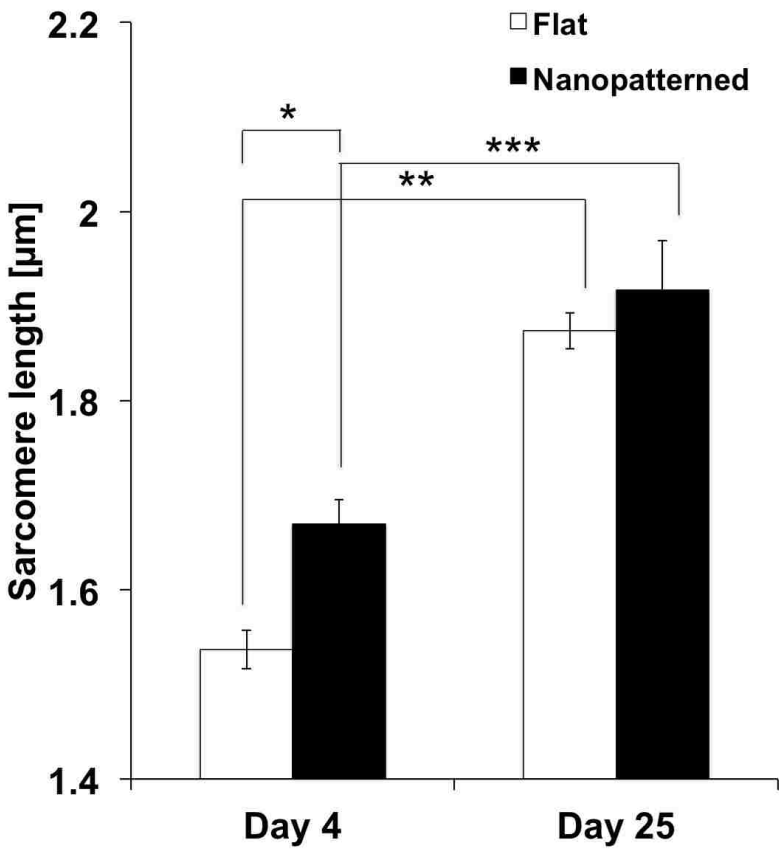

Figure 15. Sarcomere lengths of NRVMs cultured on different substrate over different periods of time measured from immunofluorescence confocal images. Sarcomere length was shown to increase over time as NRVM matures. There was a greater sarcomere length on nanopatterned cantilevers than on flat cantilevers (N=3; error bars: ± SEM; *p = 0.0002; **p < 0.0001; ***p = 0.002).

CHAPTER 4: CASE STUDIES WITH HESC-CMS AND CARDIOTOXIC COMPOUNDS

4.1 Introduction

In this study, we would investigate our previously developed system's responses to cardiotoxic compounds. Specifically, H7- and RUES2-CMs were cultured on both flat and nanopatterned PDMS cantilevers and isoproterenol, a positive chronotrope, and verapamil, a negative chronotrope, were introduced. The endpoints of this study were to characterize the effects (positive and negative chronotropic effects) of drugs on cantilevers. Moreover, the deflection measurement over time could improve our understanding of the relationship between cardiomyocyte development and contractile properties. We hypothesized that the nanopatterned cantilevers would produce greater contraction stresses than flat cantilevers as a result of better recapitulation of native myocardium structures. We also hypothesized that the cantilevers would respond to the cardiotoxic compounds according to their chronotropic and ionotropic properties. The study could provide us insights to how our system would behave in other cardiotoxic drugs bringing it closer to potential clinical application.

4.2 Materials and Methods

4.2.1 Cantilever Device Preparation

The pre-laser cut devices were made as described in chapter 2. They were chemically modified and coated with fibronectin as described. Laser cut was performed with the same procedures and settings as described in chapter 2. The PDMS filling were

adhered with the cantilever devices by pressing the PDMS side of cantilever device together with the bottom of PDMS filling. The adhered parts were then loaded into sterile 35-mm petri dishes or a 6-well plate.

4.2.2 RUES2-CM Differentiation, Seeding, and Culture

Human embryonic cell line, RUES2, was used for generating cardiomyocytes. Cardiac differentiation was accomplished using an established protocol. Replated RUES2 cells were induced with RPMI Medium 1640 (Gibco) supplemented with B-27 (Gibco) plus supplemental 100 ng/mL of activin A. After 24 hours the activin A containing medium was replaced with RPMI/B27 with supplemental BMP-4 and cultured for 4 days without medium change. At day 5, the BMP-4 containing medium was replaced with RPMI/B27 medium. After day 5 cells are fed with RPMI/B27 medium every other day and monitored for spontaneous beating activity, which peaked around day 14. The differentiated cardiomyocytes were then fed until replating for cantilever experiments between days 18 and 20. Prior to RUES2-CM seeding, the PDMS was modified as previously described and coated with fibronectin. RUES2-CMs were replated to cantilever devices using plating medium containing RPMI/B27, 10% FBS, and 1:1000 ROCK inhibitor to minimize apoptosis. Cells were seeded at 150,000 cells/cm^2. Culture was maintained in incubator at 37 °C and 5% CO_2. Medium was changed every 48 hours until further procedures. Cell attachment and growth was monitored with optical microscope (TS100F, Nikon) daily. Phase-contrast images and videos were taken with the optical microscope.

4.2.3 H7-CM Differentiation, Seeding, and Culture

Human embryonic cell line, H7, was used for generating cardiomyocytes. Cardiac differentiation was accomplished using an established protocol[63]. Cells were differentiated similar to RUES2 cardiac differentiation with the addition of 5 ng/mL bFGF between day 1 to day 4, 10 ng/mL of VEGF between day 4 to 8 and both between day 8 to 14. The differentiated cardiomyocytes were then fed until replating for cantilever experiments between days 18 and 20. Prior to H7-CM seeding, the PDMS was modified as previously described and coated with fibronectin. H7-CMs were replated to cantilever devices using plating medium containing RPMI/B27, 10% FBS, and 1:1000 ROCK inhibitor to minimize apoptosis. Cells were seeded at 150,000 cells/cm^2. Culture was maintained in incubator at 37 °C and 5% CO_2. Medium was changed every 48 hours until further procedures. Cell attachment and growth was monitored with optical microscope (TS100F, Nikon) daily. Phase-contrast images and videos were taken with the optical microscope.

4.2.4 H7-CM Cantilever Stress Quantification and Drug Experiments

7 days after replating the H7-CMs onto cantilever devices, the samples were allowed to cool down to 32°C in biosafety cabinet allowing the PNIPAM layer to dissolve thus releasing the cantilever. A pair of tweezers was used to peel the outer edge of the cantilevers. The microscope in the tissue culture room in our lab did not have objective low enough to fit the entire cantilever in the field of view. Instead, videos were recorded using an optical microscope (Axio Vert.A1, Zeiss) with 2.5x objective at the Tom & Sue Ellison Stem Cell Core. As the cantilever deflected, the tip of the cantilever quickly went

out of focus; therefore, the position of cantilever tip was approximated. The cantilever projection was manually tracked using Icy (Institut Pasteur). Specifically, the positions of the tip of the projection at the horizontal mid-line of cantilevers were tracked (**Figure 16B**). Based on the position of the base of the cantilever (at the horizontal mid-line), projection length was calculated (**Figure 16E**). The projection length was then converted to cantilever radius of curvature[67] assuming that the deformation of the cantilever was described by the arc of a circle (**Figure 16C and 17**). The radius of curvature was then used to calculate the cantilever stress using a modified Stoney's equation with the assumption of a uniform stress distribution[68] (**Figure 16D**). All the calculation was done with custom-made codes in MATLAB (MathWorks) and the equations[47,68] are as followed:

$$x = \begin{cases} Rsin(\frac{L_0}{R}) & x > \frac{L_0}{\pi} \\ R & x \geq \frac{L_0}{\pi} \end{cases}$$

$$\sigma_{cell} = \frac{Et_s^2}{6(1-\nu^2)Rt_c(1+\frac{t_c}{t_s})}$$

where x is the projection length; L_0 is the length of the cantilever; R is the radius of curvature of cantilever; σ_{cell} is the stress of the hypothetical cell layer; E, v, and t_s are the Young's modulus, Poisson's ratio, and thickness of PDMS layer, respectively; t_c is cell layer thickness (E = 2050000 Pa[69]; t_s = 0.00002 m[57]; v = 0.5[69]; t_c = 0.000005 m[70]). Systolic and diastolic stresses were quantified by taking the average of all maxima and minima of contractions, respectively. Twitch stress was the difference between systolic and diastolic stresses. Beating rate was the number of total cantilever contractions in a

given amount of time in beats per minutes (bpm).

For drug experiments, a baseline video of 20 to 30 seconds was first recorded. The same amount of drug-dosed RPMI/B27 medium with either 0.02 μM isoproterenol hydrochloride (Sigma-Aldrich)[71,72] or 0.2 μM verapamil hydrochloride (Tocris)[40,71] was added to the experimental samples doubling the total medium volume. This gave a final concentration of 0.01 μM isoproterenol or 0.1 μM verapamil. It has been shown that beating of the cells could be interrupted by compound addition and that the best stability of cell beating occurred approximately after 5 min after the addition[71]. Both control and experimental samples were put back into the incubator in 5 min intervals. At 5, 10, and 15 min, videos were recorded. After drug infusion experiment, old medium was replaced with fresh medium and the samples were incubated for 5 min. Again, old medium was replaced with fresh medium and the samples were put back into the incubator.

4.2.5 RUES2-CM Cantilever Stress Quantification and Drug Experiments

7 days after replating RUES2-CMs onto cantilever devices, the samples were allowed to cool down to 32 °C in biosafety cabinet allowing the PNIPAM layer to dissolve thus releasing the cantilever. A pair of tweezers was used to peel the outer edge of the cantilevers. Once the cantilevers were free to bend, the samples were loaded onto the stereoscope (Stereomaster, Cat. No 12563411, Fisher). An iPhone-microscope adaptor (HookUpZ, Carson) was attached to the stereoscope along with an iPhone 5 (Apple) (**Figure 16A**). Videos were taken with the iPhone and were later imported and converted into .avi on a computer. The .avi videos were converted into gray scale and the projection of the top of the cantilevers was enhanced by increasing the contrast

(**Figure 16B**). The cantilever projection was manually tracked using Icy (Institut Pasteur) (**Figure 16B**). Specifically, the positions of the tip of the projection at the horizontal mid-line of cantilevers were tracked. Based on the position of the base of the cantilever (at the horizontal mid-line), projection length was calculated (**Figure 16E**). The projection length over each frame was then converted to cantilever radius of curvature[67] assuming that the deformation of the cantilever was described by the arc of a circle (**Figure 16C and 17**). The radius of curvature was then used to calculate the cantilever stress using a modified Stoney's equation with the assumption of a uniform stress distribution[68] (**Figure 16C and 16D**). All the calculation was done with custom-made codes in MATLAB (MathWorks) as described previously.

For the drug experiment, a baseline video was first recorded. The same amount of fresh RPMI/B27 medium was added to control sample doubling the total medium volume. The same amount of drug-dosed RPMI/B27 medium with 0.02 μM isoproterenol hydrochloride (Sigma-Aldrich)[71,72] was added to the experimental samples doubling the total medium volume. This gave a final concentration of 0.01 μM isoproterenol. Both control and experimental samples were put back into the incubator in 5 min intervals. At 5, 10, and 15 min, videos were recorded. After drug infusion experiment, old medium was replaced with fresh medium and the samples were incubated for 5 min. Again, old medium was replaced with fresh medium and the samples were put back into the incubator. Cantilever stress quantification was carried out. Systolic and diastolic stresses were quantified by taking the average of all maxima and minima, respectively. Twitch stress was the difference between systolic and diastolic stresses. Beating rate

was the number of total cantilever contractions in a given amount of time in beats per minutes (bpm).

4.2.6 Statistical Analysis

All data are presented as mean ± SEM unless otherwise specified. Student's t-test was used to evaluate the statistical significance. Significance level was set at $p<0.05$.

4.3 Results and Discussion

4.3.1 H7-CM Cantilevers

H7-CMs were able to form a uniform monolayer and beat spontaneously 3 days after replating onto cantilevers. H7-CMs were allowed to develop over the next 7 days for optimal contraction. At day 10, problems with releasing laser-cut cantilevers were encountered as a result of cells growing over the cut. Laser cutting was performed prior to fibronectin coating in this H7-CM study. We decided to create cantilevers manually using scalpel. On the same day immediately after the cuts were performed, H7-CMs stopped beating due to damages caused by the cut. One day after the cut (day 11), cells recovered from the cut and beating on both flat (twitch: 1.38(± 0.058) kPa; systolic: 12.09(± 0.037) kPa; diastolic: 10.71(± 0.045) kPa) and nanopatterned (twitch: 6.086(± 0.090) kPa; systolic: 14.50(± 0.089) kPa; diastolic: 8.41(± 0.010) kPa) cantilevers was observed (**Figure 18 and 19**). The higher stresses produced in the nanaopatterned cantilever could be caused by the alignment of cardiomyocytes itself. Aligned cardiomyocytes would create a stronger contraction along the direction of nanopattern

comparing to contraction traversing the direction of nanopattern.

Drug experiments were then performed on 12 and 13 days post cardiomyocyte replating. However, the cell layer was completely detached from the nanopatterned cantilevers making stress quantification impossible. Drug studies were done only with the flat cantilever. On day 12, isoproterenol was introduced to the culture and videos were recorded. Before the drug treatment, a baseline recording was performed. 22.07(± 0.23) kPa at systolic stress, 13.01(± 0.20) kPa at diastolic stress, and 9.073(± 0.31) kPa at twitch stress were observed. As expected, significant increases in beating rate was observed immediately after introduction of isoproterenol (**Figure 20 and 23**). This increase could be explained by the activation of β1-adrenoreceptor on myocardial cells by isoproterenol. Theoretically, this would increase the conduction velocity of action potential, increasing both beating rate and contractile force[73]. However, a decrease in contractile stress was observed (**Figure 20 and 22**). Specifically, the twitch stress remained significantly lower than that of baseline even 15 minutes after isoproterenol treatment (**Figure 22A**). The same reduction was observed in systolic stress (**Figure 22B**). Greater beating rates compared to that of baseline were maintained even the rate slowly recovered over the 15-minute period (**Figure 23**). Isoproterenol was washed out overnight and verapamil experiments were performed the next day.

Verapamil is an L-type calcium channel blocker. It slows action potential conduction and decrease spontaneous beating. Before the drug treatment, a baseline recording was performed. 34.22(± 0.28) kPa at systolic stress, 14.59(± 0.14) kPa at diastolic stress, and 19.64(± 0.31) kPa at twitch stress were observed. Unexpectedly,

the beating rate of cells increased (**Figure 21 and 23**) while contractile stress decreased (**Figure 21 and 22**). Significant decreases in twitch, systolic, and diastolic stresses were observed but they slowly recovered over the 15-minute period (**Figure 22**). There was a sharp increase in beating rate immediately after verapamil introduction. However, unlike isoproterenol, the beating rate quickly recovered to near-baseline level 10 minutes after verapamil treatment (**Figure 23**).

It is important to note that there was a universal increase in contractile stresses over the 3 days of cantilever experiments, possibly, as a result of H7-CMs recovering from the cut from day 10 (**Figure 18 and 22**). However, in both drug experiments, an increase in beating rate and a decrease in contractile stresses were observed immediately after drug introduction. The results did not match up with our expectations and could be explained by the limitations of these studies. First, manual cutting was very destructive and cantilevers produced were rarely reproducible. Second, gradual cell detachment was observed starting from day 7. The detachment could cause a non-uniform layer of cells making the stress quantification less accurate. Third, the drug experiments were done without a control for the addition of new medium. The lack of control could complicate the outcomes from the effects of medium addition with the actual effects of drugs.

4.3.2 RUES2-CM Cantilevers

RUES2-CMs were cultured on laser-cut cantilevers. We were able to get proper cell adhesion 3 days after replating onto cantilevers. Cells started to clump up and detach from the cantilevers from day 6, so we decided to release the cantilevers on the same

day. On day 6, minimal cantilever deflection was observed due to RUES2-CMs' early stage in culture. On day 11, stronger cantilever deflections and robust rhythmic contractions were observed possibly due to maturation of cardiomyocytes over time (**Figure 24**). It is, however, important to note that cell detachment from the cantilevers intensified after day 6. Drug experiments were performed on day 8, 16, and 17; however, due to cell clumps and uneven cell layer, the cantilevers were deformed in different directions. The shape of these RUES2-CM cantilevers did not represent an arc of circle by day 11. Therefore, our methods would not no longer be able to accurately quantify the cantilever stress.

4.4 Summary

Here we utilized cantilevers for studying the effects of known cardiotoxic compounds on hESC-CMs. This study investigated the stress generation of the cells by analyzing the deflection of cantilevers. We found that H7-CMs were able to maintain a monolayer until damage to tissue was made by manual cutting. RUES2-CMs were not able to maintain a monolayer after day 6. Quantification of cell layer stress was performed and cardiomyocyte responses were observed when isoproterenol and verapamil were introduced. As expected, the nanopatterned cantilever produced greater contractile stresses than flat cantilevers. We suggested the greater contractile stresses were the results of better-aligned cardiomyocytes on the nanopatterned cantilevers. The cantilevers' responses to cardiotoxic compounds did not agree with our expectations. We were not able to judge the exact reason behind this disagreement due to the lack of

control for medium addition. We postulated that the introduction of medium disturbed cardiomyocytes and reduced cell contraction. However, the effects of drugs became more apparent as cells recovered from perturbation over time. On the other hand, a more physiological stress was produced by cardiomyocytes as they remained on cantilevers over time. We postulated the increase in contraction stresses over time was a result of cardiomyocyte recovery from perturbation. We were not able to compare the effects of cardiotoxic compounds on flat and nanopatterned cantilevers due to complete cell detachment or significant cell clumping on the nanopatterned cantilevers. We demonstrated the ability of cantilevers in detecting the quality of cell monolayer on cantilevers and cardiomyocytes' responses to cardiotoxic compounds over time.

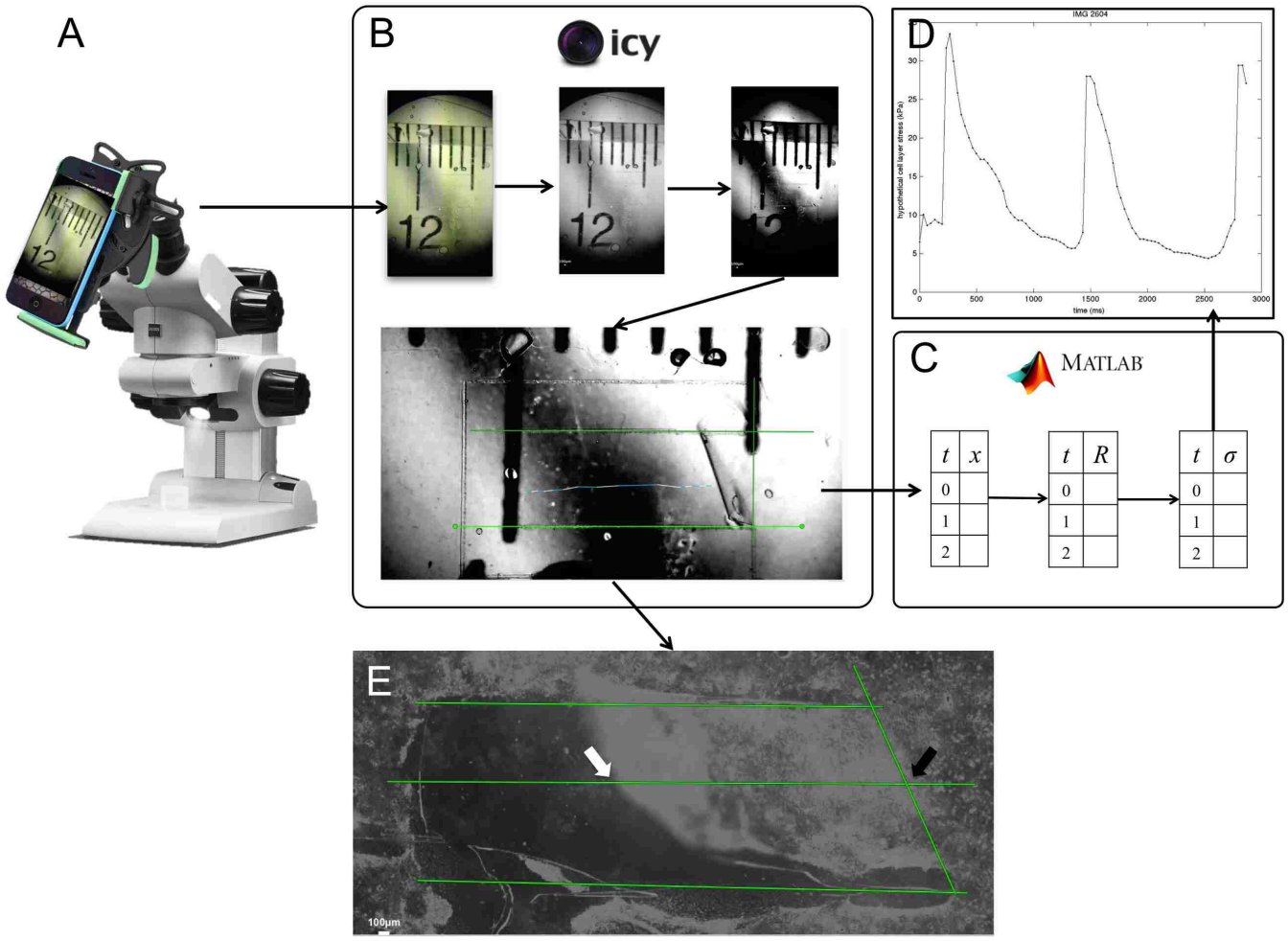

Figure 16. A flow chart showing how stress quantification was performed. Black thin arrows indicate direction of information flow. (A) Videos were recorded using an iPhone attached to a stereoscope. (B) Videos were imported into Icy, converted into gray scale, and enhanced by increasing the contrast. Manual tracking of the tip of the projection was performed. (C) Projection length, x, as a function of time, t, was converted into radius of curvature, R, then cantilever stress, σ, in MATLAB. (D) Cantilever stress was plotted against time to visualize the data. (E) Projection length of cantilever was calculated by finding the distance between tip position (white arrow) and base position (black arrow) which were manually identified.

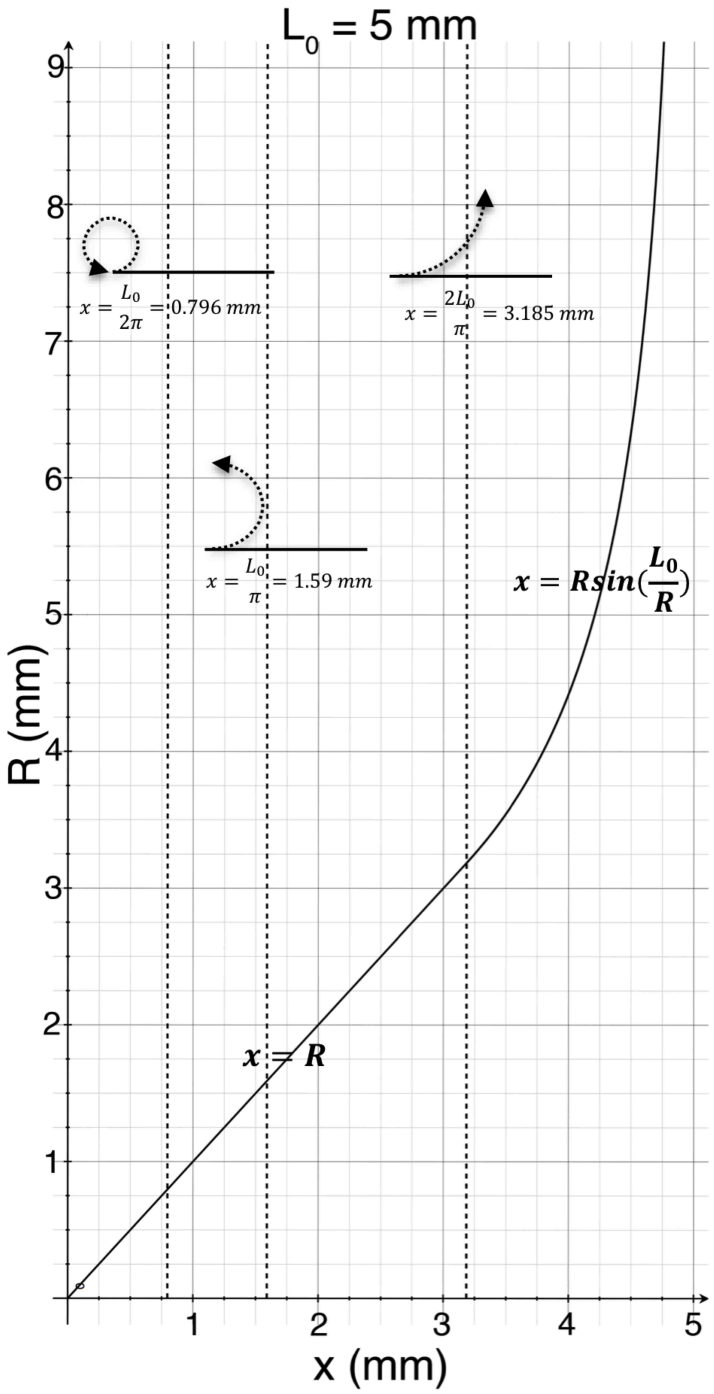

Figure 17. Graph of radius of curvature, R, of a cantilever as a function of projection length, x. Three phases of cantilever deflection are visualized at x = 0.796, 1.59, and 3.185 mm. At x = 0.796 mm, a full circle is formed. At x = 1.59 mm, half of a circle is formed. At x = 3.185 mm, a quarter of a circle is formed. When x is less than or equal to 3.185 mm, x=R is used to calculate R. It is important to note that a different equation is used when x is greater than 3.185 mm.

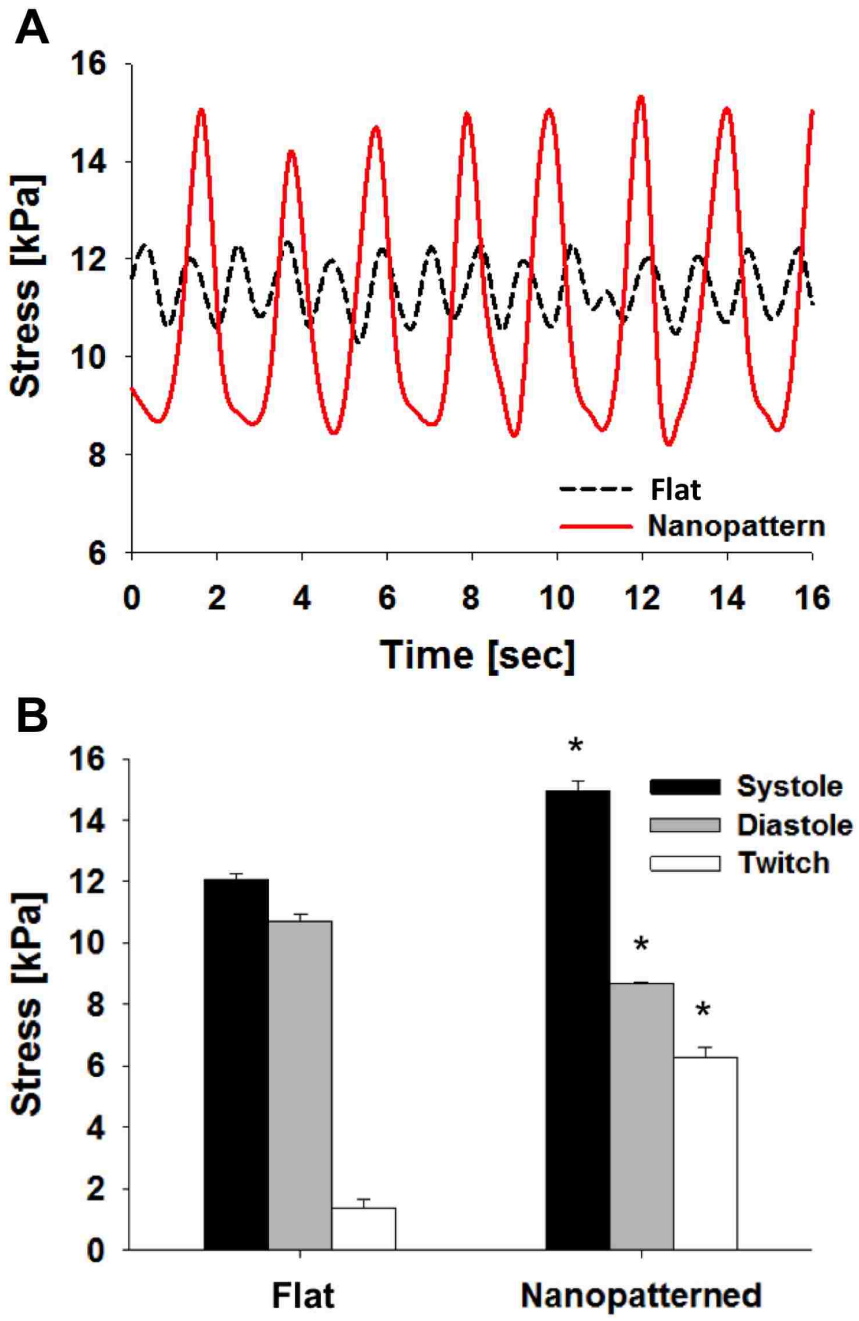

Figure 18. Quantification of H7-CM flat and nanopatterned cantilevers cell layer stress on day 11. (A) H7-CM twitch stress over time on both flat and nanopatterned cantilevers created with manual cutting at day 11. (B) The twitch, systolic, and diastolic stresses of flat and nanopatterned cantilever with H7-CMs. On day 11, the nanopatterned cantilever produced greater twitch, systolic, and diastolic stresses than the flat cantilever (error bar: ± SEM; * $p < 0.0001$)

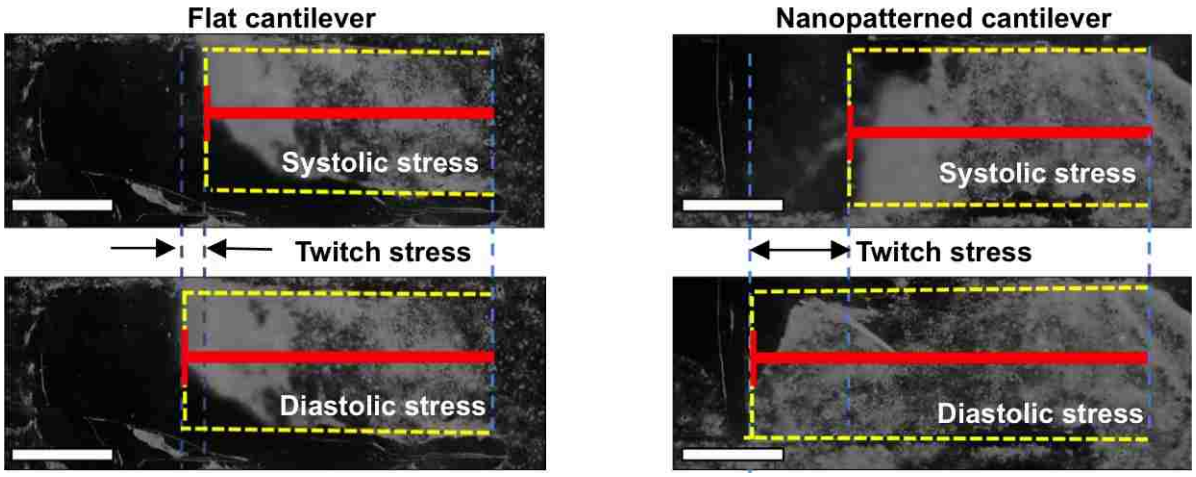

Figure 19. Schematics showing greater twitch stress observed using nanopatterned cantilevers. Quantification of H7-CM flat and nanopatterned cantilevers cell layer stress on day 11. Still images from video recordings of the motion H7-CMs on cantilever. The motions were captured 11 days after plating cells. Scale bars: 1 mm

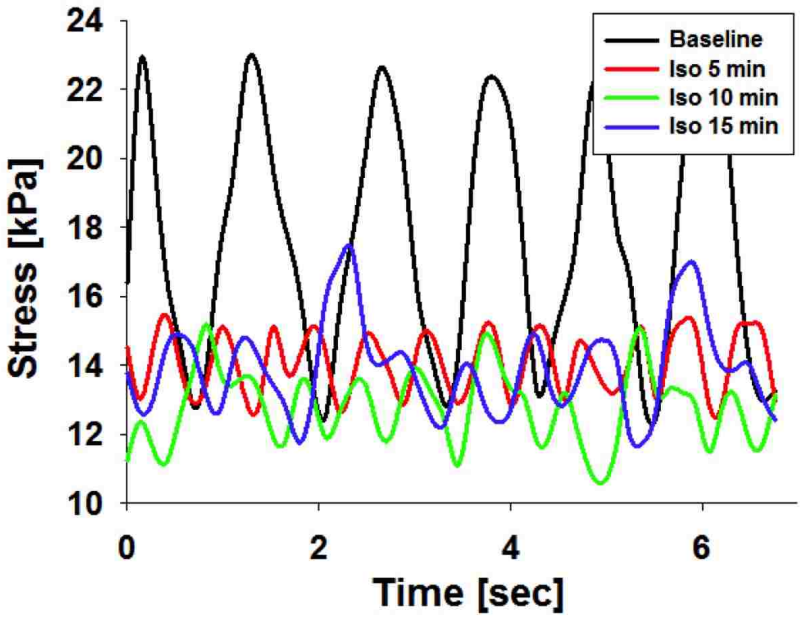

Figure 20. H7-CM stress of flat cantilever before and after isoproterenol treatment on day 12. H7-CM stress plotted over time before isoproterenol treatment and 5, 10, and 15 minutes after treatment. Contraction stress was greatly reduced after treatment as shown by the difference between baseline contraction and treatment contractions.

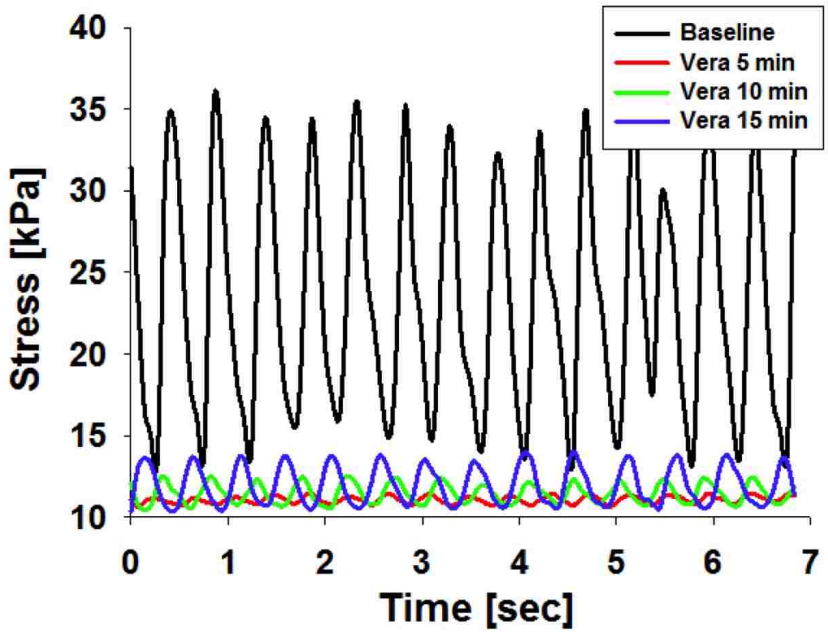

Figure 21. H7-CM stress of flat cantilever before and after verapamil treatment on day 13. H7-CM stress plotted over time before verapamil treatment and 5, 10, and 15 minutes after treatment. Contraction stress was greatly reduced after treatment as shown by the difference between baseline contraction and treatment contractions.

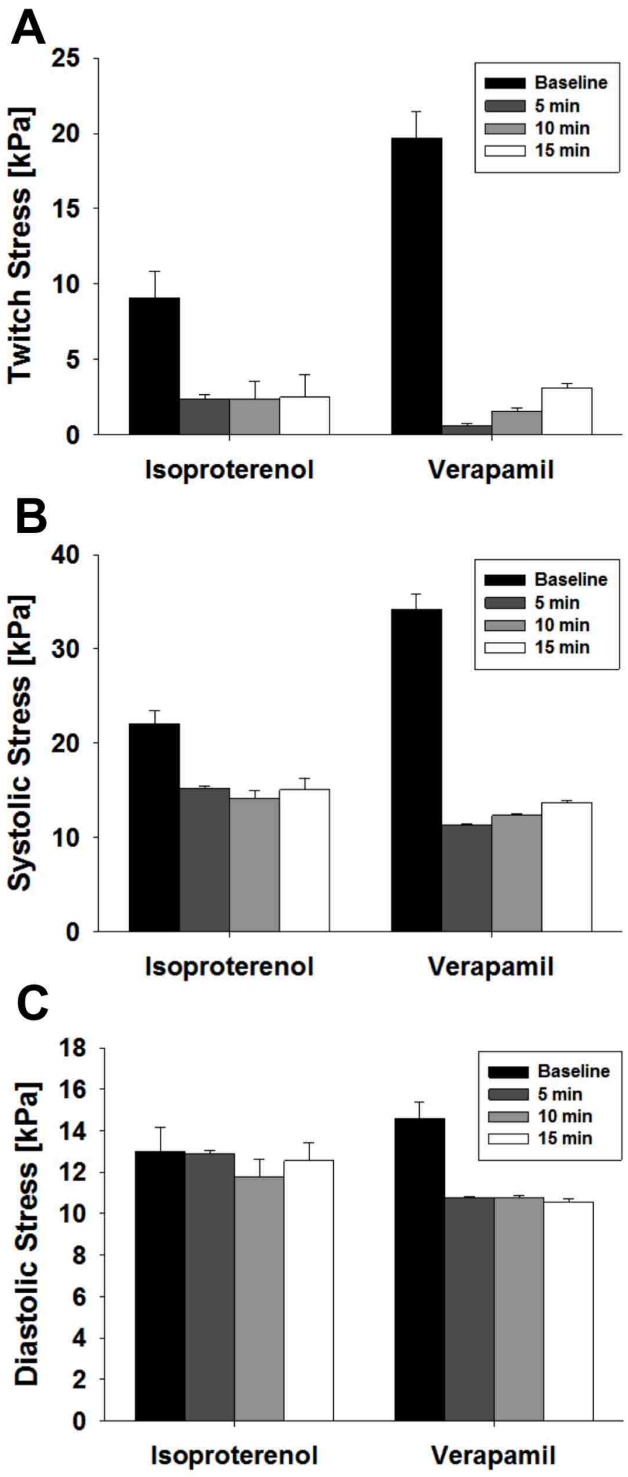

Figure 22. Contractile stresses of H7-CM cells on flat cantilever before and after drug treatments. (A) The twitch stress calculated as the difference between systolic stress and diastolic stress. (B) Systolic stress as the average of the maxima stresses recorded during cantilever contraction. (C) Diastolic stress as the average of the minima stresses recorded during cantilever contraction (error bar: ± SD).

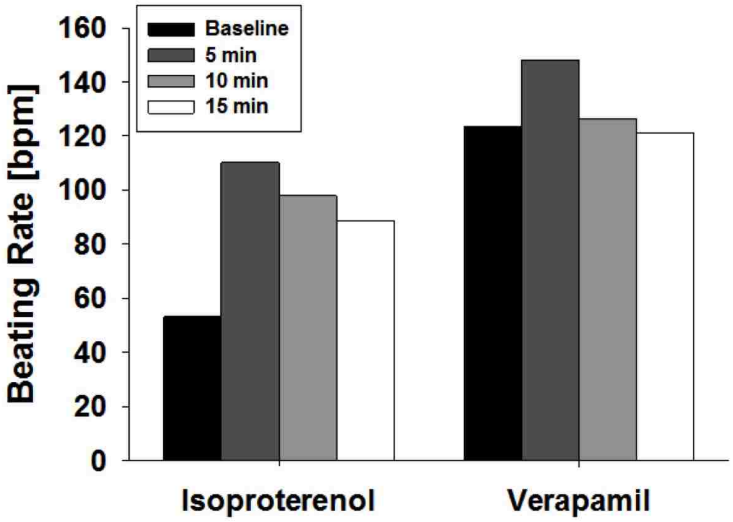

Figure 23. Beating rate of H7-CMs on flat cantilever before and after drug treatments. Beating rate calculated as the total number of beats recorded over the length of the recording. An increase in contraction rate after drug treatment was universal. A slow recovery of contraction rate over 15 minutes after each treatment was observed as well.

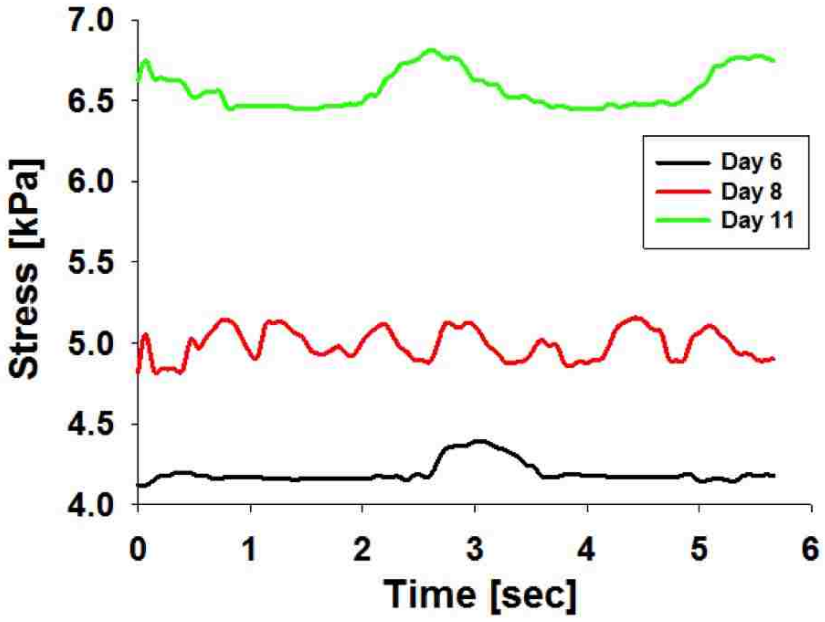

Figure 24. Increase in RUES2-CM cell layer stress over a period of 6 days. A gradual increase in cell layer stress was observed from day 6 to day 11. A change in contraction pattern was also observed. This could be due to the maturation of RUES2-CMs over time. This effect was also observed with H7-CMs from day 11 to day 13.

CHAPTER 5: CONCLUSIONS

In this study, we reported the development of a device for assaying contractile properties of stem cell-derived cardiomyocytes made of nanopatterned PDMS cantilevers. First, we optimized the production of the assay by fabricating cantilevers using different spin coating setting and curing methods. The thickness and topography were characterized using SEM and optical microscope. We were able to produce PDMS cantilevers of a thickness of 20 μm and topography made of 800 nm ridges and grooves. The thickness of cantilevers produced agreed with the literatures. The nanopattern of the cantilevers was made to resemble the nanotopography of native human myocardium in order to induce optimal cardiomyocyte development. We validated enhanced cell adhesion on chemically modified PDMS substrates. The release of cantilevers was also optimized so that cells remained untouched and attached. In the second part of the study, we developed and validated the ability of cantilevers to support development of cardiomyocytes. Alignment of cell and cytoskeleton and increased cell elongation and sarcomere length were observed on nanopatterned cantilevers validating enhanced structural maturation. The improved structural maturation demonstrated was in agreement with previous studies done by Kim *et al*. Last, we demonstrated the ability of our cantilever devices to evaluate contractile properties of cardiomyocytes such as twitch, systolic, diastolic stresses. We created cantilevers with hESC-CMs and introduced known cardiotoxic compounds. Greater contractile stresses were observed using nanopatterned cantilever verifying our hypothesis. However, the responses to cardiotoxic compounds disagreed with our expectations. We were not able

to deduce the reason behind the disagreement due to the lack of controls for medium addition. Moreover, an increase in cantilever stress was observed over time as cardiomyocytes recovered from physical perturbation. There could also be a possibility that cardiomyocytes matured over time potentially validating the relationship between structural maturation and cantilever stress.

With better cellular and cytoskeletal alignments, greater contractile stresses were observed using the nanopatterned cantilever comparing to flat cantilever. The enhanced contractile stresses validated our hypothesis that nanopatterned cantilevers could better recapitulate the contractile properties of native human myocardium. However, we were not able to compare the performance of nanopatterned and flat cantilevers in assaying cardiotoxic compounds as a result of significant cell detachment. Overall, the results demonstrated our system's ability to quantify more physiologically relevant contractile properties of cardiomyocytes.

As compared with previous studies that used μCP thin films, we were able to create a more physiologically accurate engineered cardiac tissue using our nanopatterning technology. This study provides a platform for future research in creating an assay that incorporates technologies, such as reduced graphene oxide (rGO) coating surface, that could further improve engineered cardiac tissue maturation. It also provides a platform for an assay that is capable of more functional measurements, such as electrophysiological characteristics.

It is important to consider the limitations of study. In our first study, even though the thickness and nanopatterned were optimized as wanted, more accurate stress

quantification could be made by performing the thickness measurements on each batch of cantilevers produced. Specifically, the thickness and elasticity of cantilevers could be performed on each batch of cantilevers fabricated. With this approach, the variation between calculated and actual cantilever stresses could be minimized. In our second study, even though cardiomyocytes were shown to align to the nanopatterns, better cell quality could further validate the enhancement in structural maturation. Specifically, the immunofluorescence images of NRVMs showed patches of cardiomyocytes instead of a monolayer of cardiomyocytes. To further validate the benefits of nanopatterns on cardiomyocyte development, studies evaluating cardiac gene expression and action potential characteristics would be required. Most importantly, the quality of stress quantification was poor due to significant cardiomyocyte detachment when prolonged cultures were carried out. Further investigation to enhance cell adhesion and monolayer formation could improve the accuracy of our assumptions used in the quantification of cantilever stress. Lastly, introduction of other known cardiotoxic compounds could further validate our system's ability in drug-induced cardiotoxicity screening.

VITA

Daniel Chen Lih was born in Columbus, Ohio and raised in Taichung, Taiwan. He earned a Bachelor's in Bioengineering from the University of Washington in 2014. He earned a Master's in Bioengineering from the University of Washington in 2016.

REFERENCES

1. Dykens JA, Will Y (2007) The significance of mitochondrial toxicity testing in drug development. *Drug discovery today 12*(17): 777-785.
2. Avorn J (2008) *Powerful medicines: the benefits, risks, and costs of prescription drugs*. Vintage.
3. Menna P, Salvatorelli E, Minotti G (2008) Cardiotoxicity of Antitumor Drugs. *Chemical research in toxicology 21*(5): 978-989.
4. Paul SM, *et al* (2010) How to improve R&D productivity: the pharmaceutical industry's grand challenge. *Nature reviews Drug discovery 9*(3): 203-214.
5. Chi KR (2013) Revolution dawning in cardiotoxicity testing. *Nature reviews Drug discovery 12*(8): 565-567.
6. Lu HR, *et al* (2008) Predicting drug - induced changes in QT interval and arrhythmias: QT - shortening drugs point to gaps in the ICHS7B Guidelines. *British journal of pharmacology 154*(7): 1427-1438.
7. Redfern WS, *et al* (2003) Relationships between preclinical cardiac electrophysiology, clinical QT interval prolongation and torsade de pointes for a broad range of drugs: evidence for a provisional safety margin in drug development. *Cardiovascular research 58*(1): 32-45.
8. Poveda F, Martí E, Gil D, Carreras F, Ballester M (2012) Helical structure of ventricular anatomy by diffusion tensor cardiac MR tractography. *JACC: Cardiovascular Imaging 5*(7): 754-755.
9. Kim DH, *et al* (2010) Nanoscale cues regulate the structure and function of macroscopic cardiac tissue constructs. *Proceedings of the National Academy of Sciences 107*(2): 565-570.
10. Prabhakaran MP, *et al* (2012) Stem cells and nanostructures for advanced tissue regeneration. In *Biomedical applications of polymeric nanofibers* (Springer Berlin Heidelberg) pp. 21-62.

11. Thubrikar MANO, Piepgrass WC, Bosher LP, Nolan SP (1980) The elastic modulus of canine aortic valve leaflets in vivo and in vitro. *Circulation research 47*(5): 792-800.
12. Ghista D N, Vayo, WH, Sandler H (1975) Elastic modulus of the human intact left ventricle—determination and physiological interpretation. *Medical and biological engineering 13*(2): 151-161.
13. Classen DC, Pestotnik SL, Evans RS, Lloyd JF, Burke JP (1997) Adverse drug events in hospitalized patients: excess length of stay, extra costs, and attributable mortality. *Jama 277*(4): 301-306.
14. Liang P, *et al* (2013) Drug screening using a library of human induced pluripotent stem cell-derived cardiomyocytes reveals disease specific patterns of cardiotoxicity. *Circulation* CIRCULATIONAHA-113.
15. Davis RP, van den Berg CW, Casini S, Braam SR, Mummery CL (2011) Pluripotent stem cell models of cardiac disease and their implication for drug discovery and development. *Trends in molecular medicine 17*(9): 475-484.
16. Zicha S, *et al* (2003) Molecular basis of species-specific expression of repolarizing K+ currents in the heart. American *Journal of Physiology-Heart and Circulatory Physiology 285*(4): H1641-H1649.
17. Marchetto MC, *et al* (2010) A model for neural development and treatment of Rett syndrome using human induced pluripotent stem cells. *Cell 143*(4): 527-539.
18. Liu H, Ye Z, Kim Y, Sharkis S, Jang YY (2010) Generation of endoderm‐derived human induced pluripotent stem cells from primary hepatocytes. *Hepatology 51*(5): 1810-1819.
19. Taura D, *et al* (2009) Induction and isolation of vascular cells from human induced pluripotent stem cells—brief report. *Arteriosclerosis, thrombosis, and vascular biology 29*(7): 1100-1103.
20. Lee YK, *et al* (2011) Calcium homeostasis in human induced pluripotent stem cell-derived cardiomyocytes. *Stem Cell Reviews and Reports 7*(4): 976-986.

21. Navarrete EG, *et al* (2013) Screening Drug-Induced Arrhythmia Using Human Induced Pluripotent Stem Cell–Derived Cardiomyocytes and Low-Impedance Microelectrode Arrays. *Circulation 128*(11 suppl 1): S3-S13.
22. Lundy SD, Zhu WZ, Regnier M, Laflamme MA (2013) Structural and functional maturation of cardiomyocytes derived from human pluripotent stem cells. *Stem cells and development 22*(14): 1991-2002.
23. Kim DH, *et al* (2012) Nanopatterned cardiac cell patches promote stem cell niche formation and myocardial regeneration. *Integrative Biology 4*(9): 1019-1033.
24. Kim DH, *et al* (2006) Guided three-dimensional growth of functional cardiomyocytes on polyethylene glycol nanostructures. *Langmuir 22*(12): 5419-5426.
25. Kim DH, Wong PK, Park J, Levchenko A, Sun Y (2009) Microengineered platforms for cell mechanobiology. *Annual review of biomedical engineering 11*: 203-233.
26. Bélanger MC, Marois Y (2001) Hemocompatibility, biocompatibility, inflammatory and in vivo studies of primary reference materials low‐density polyethylene and polydimethylsiloxane: A review. *Journal of biomedical materials research 58*(5): 467-477.
27. Zhou J, Ellis AV, Voelcker NH (2010) Recent developments in PDMS surface modification for microfluidic devices. *Electrophoresis 31*(1): 2-16.
28. Zhou J, Khodakov DA, Ellis AV, Voelcker NH (2012) Surface modification for PDMS‐based microfluidic devices. *Electrophoresis 33*(1): 89-104.
29. Wang L, Sun B, Ziemer KS, Barabino GA, Carrier RL (2010) Chemical and physical modifications to poly (dimethylsiloxane) surfaces affect adhesion of Caco‐2 cells. *Journal of biomedical materials research Part A 93*(4): 1260-1271.
30. Wittmer CR, Phelps JA, Saltzman WM, Van Tassel PR (2007) Fibronectin terminated multilayer films: protein adsorption and cell attachment studies. *Biomaterials 28*(5): 851-860.

31. Toworfe GK, Composto RJ, Adams CS, Shapiro IM, Ducheyne P (2004) Fibronectin adsorption on surface‐activated poly (dimethylsiloxane) and its effect on cellular function. *Journal of Biomedical Materials Research Part A 71*(3): 449-461.
32. Odom TW, Love JC, Wolfe DB, Paul KE, Whitesides GM (2002) Improved pattern transfer in soft lithography using composite stamps. *Langmuir 18*(13): 5314-5320.
33. Choi KM, Rogers JA (2003) A photocurable poly (dimethylsiloxane) chemistry designed for soft lithographic molding and printing in the nanometer regime. *Journal of the American Chemical Society 125*(14): 4060-4061.
34. Schmid H, Michel B (2000) Siloxane polymers for high-resolution, high-accuracy soft lithography. *Macromolecules 33*(8): 3042-3049.
35. Mills KL, Zhu X, Takayama S, Thouless MD (2008) The mechanical properties of a surface-modified layer on polydimethylsiloxane. *Journal of materials research 23*(01): 37-48.
36. Fuard D, Tzvetkova-Chevolleau T, Decossas S, Tracqui P, Schiavone P (2008) Optimization of poly-di-methyl-siloxane (PDMS) substrates for studying cellular adhesion and motility. *Microelectronic Engineering 85*(5): 1289-1293.
37. Kim HN, *et al*. (2012) Patterning methods for polymers in cell and tissue engineering. *Annals of biomedical engineering 40*(6): 1339-1355.
38. Lan F, *et al* (2013) Abnormal calcium handling properties underlie familial hypertrophic cardiomyopathy pathology in patient-specific induced pluripotent stem cells. *Cell stem cell 12*(1): 101-113.
39. Himmel HM (2013) Drug-induced functional cardiotoxicity screening in stem cell-derived human and mouse cardiomyocytes: effects of reference compounds. *Journal of pharmacological and toxicological methods 68*(1): 97-111.
40. Sirenko O, *et al* (2012) Multiparameter in vitro assessment of compound effects on cardiomyocyte physiology using iPSC cells. *Journal of biomolecular screening* 1087057112457590.

41. You J, *et al* (2014) Cardiomyocyte sensor responsive to changes in physical and chemical environments. *Journal of biomechanics 47*(2): 400-409.
42. Feinberg AW, *et al* (2007) Muscular thin films for building actuators and powering devices. *Science 317*(5843): 1366-1370.
43. Alford PW, Feinberg AW, Sheehy SP, Parker KK (2010) Biohybrid thin films for measuring contractility in engineered cardiovascular muscle. *Biomaterials 31*(13): 3613-3621.
44. McCain ML, Agarwal A, Nesmith HW, Nesmith AP, Parker KK (2014) Micromolded gelatin hydrogels for extended culture of engineered cardiac tissues. *Biomaterials 35*(21): 5462-5471.
45. Grosberg A, *et al* (2012) Muscle on a chip: in vitro contractility assays for smooth and striated muscle. *Journal of pharmacological and toxicological methods 65*(3): 126-135.
46. Feinberg AW, *et al* (2012) Controlling the contractile strength of engineered cardiac muscle by hierarchal tissue architecture. *Biomaterials 33*(23): 5732-5741.
47. Grosberg A, Alford PW, McCain ML, Parker KK (2011) Ensembles of engineered cardiac tissues for physiological and pharmacological study: heart on a chip. *Lab on a chip 11*(24): 4165-4173.
48. Agarwal A, Goss JA, Cho A, McCain ML, Parker KK (2013) Microfluidic heart on a chip for higher throughput pharmacological studies. *Lab on a Chip 13*(18): 3599-3608.
49. Sheehy SP, Pasqualini F, Grosberg A, Park SJ, Aratyn-Schaus Y, Parker KK (2014) Quality metrics for stem cell-derived cardiac myocytes. *Stem cell reports 2*(3): 282-294.
50. Feinberg AW, et al (2013) Functional differences in engineered myocardium from embryonic stem cell-derived versus neonatal cardiomyocytes. *Stem cell reports 1*(5): 387-396.
51. Zhang B, Xiao Y, Hsieh A, Thavandiran N, Radisic M (2011) Micro-and nanotechnology in cardiovascular tissue engineering. *Nanotechnology 22*(49): 494003.

52. Schift H, *et al* (2005) Controlled co-evaporation of silanes for nanoimprint stamps. *Nanotechnology 16*(5): S171.
53. Xia Y, Whitesides GM (1998) Soft lithography. *Annual review of materials science 28*(1): 153-184.
54. Yanker DM, Maurer JA (2008) Direct printing of trichlorosilanes on glass for selective protein adsorption and cell growth. *Molecular Biosystems 4*(6): 502-504.
55. Tourovskaia A, Figueroa-Masot X, Folch A (2005) Differentiation-on-a-chip: a microfluidic platform for long-term cell culture studies. *Lab on a Chip 5*(1): 14-19.
56. Fisher AK, Brian WB (2011) Cell Growth Protocol and Differentiation treatment for the C2C12 Cell Line. *Wold mouse ENCODE*.
57. Casquillas GV, Berre ML, Terriac E, Bertholle F PDMS thickness VS spin‐coating speed. http://www.elveflow.com/
58. Kim J, *et al* (2008) Quantitative evaluation of cardiomyocyte contractility in a 3D microenvironment. *Journal of biomechanics 41*(11): 2396-2401.
59. Kim HN, *et al* (2013) Nanotopography-guided tissue engineering and regenerative medicine. *Advanced drug delivery reviews 65*(4): 536-558.
60. Lundy SD, Zhu WZ, Regnier M, Laflamme MA (2013) Structural and functional maturation of cardiomyocytes derived from human pluripotent stem cells. *Stem cells and development 22*(14): 1991-2002.
61. Boateng SY, *et al* (2003) Inhibition of fibroblast proliferation in cardiac myocyte cultures by surface microtopography. *American Journal of Physiology-Cell Physiology 285*(1): C171-C182.
62. Toraason M, Luken ME, Breitenstein M, Krueger JA, Biagini RE (1989) Comparative toxicity of allylamine and acrolein in cultured myocytes and fibroblasts from neonatal rat heart. *Toxicology 56*(1): 107-117.
63. Sa S, McCloskey KE (2012) Stage-specific cardiomyocyte differentiation method for H7 and H9 human embryonic stem cells. *Stem Cell Reviews and Reports 8*(4): 1120-1128.
64. C-Pace EP Culture Stimulator for Chronic Pacing. http://www.ionoptix.com/product/cell-culture-pacing/

65. Yamasaki KI, *et al* (2009) Control of myotube contraction using electrical pulse stimulation for bio-actuator. *Journal of Artificial Organs 12*(2): 131-137.
66. Akiyama Y, Furukawa Y, Morishima K (2006) Controllable bio-microactuator powered by muscle cells. In *IEEE Int Conf Engineering in Medicine and Biology* pp. 6565-6568.
67. Shim J, Grosberg A, Nawroth JC, Parker KK, Bertoldi K (2012) Modeling of cardiac muscle thin films: pre-stretch, passive and active behavior. *Journal of biomechanics 45*(5): 832-841.
68. Wang G, *et al* (2014) Modeling the mitochondrial cardiomyopathy of Barth syndrome with induced pluripotent stem cell and heart-on-chip technologies. *Nature medicine 20*(6): 616-623.
69. Johnston ID, McCluskey DK, Tan CKL, Tracey MC (2014) Mechanical characterization of bulk Sylgard 184 for microfluidics and microengineering. *Journal of Micromechanics and Microengineering 24*(3): 035017.
70. Luo D, *et al* (2008) Nuclear Ca 2+ sparks and waves mediated by inositol 1, 4, 5-trisphosphate receptors in neonatal rat cardiomyocytes. *Cell calcium 43*(2): 165-174.
71. Butler L, *et al* (2015) Enhanced characterization of contractility in cardiomyocytes during early drug safety assessment. *Toxicological Sciences 145*(2): 396-406.
72. Pointon A, Abi-Gerges N, Cross MJ, Sidaway JE (2013) Phenotypic profiling of structural cardiotoxins in vitro reveals dependency on multiple mechanisms of toxicity. *Toxicological sciences 132*(2): 317-326.
73. Piascik MT, Perez DM (2001) α1-Adrenergic receptors: new insights and directions. *Journal of Pharmacology and Experimental Therapeutics 298*(2): 403-410.